Synthesis And Optical and Structural Characterization Of Pure α: PbO and Sn and Co-Doped α: PbO

A THESIS PRESENTED TO
THE PROGRAM OF GRADUATE STUDIES
ADDIS ABABA UNIVERSITY
IN PARTIAL FULFILLMENT OF THE REQUIREMENTS
FOR THE DEGREE
MASTER OF SCIENCE IN PHYSICS
(Polymer Physics)

By

Alehegn Bazezew

Advisor

Fekadu Gashaw (Professor)

Addis Ababa, Ethiopia

Augest 2024

ADDIS ABABA UNIVERSITY

PROGRAM OF GRADUATE STUDIES

COLLEGE of NATURAL and COMPUTATIONAL SCIENCES

DEPARTMENT of PHYSICS

This is to certify that the thesis prepared by AlehegnBazezewTegegne under the title: Synthesizing, Characterizing and Studying Structural and Optical Properties of Pure α: PbO, Sn: α: PbO and Co: α: PbO Prepared By Co-Pricptation Method for the Degree of Master of Science (M.Sc) in Physics compiles with regulation of the university and meets the accepted standards with respect to originality and quality.

Dated: Augest 2024

Approved by the Examining Committee:

Prof. Fekadu Gashaw **Signature** _____Date____/____/___

Advisor

_____ **Signature** _____Date____/____/___

Examiner

_____ **Signature** _____Date____/____/___

Examiner

ADDIS ABABA UNIVERSITY

Date: **Augest 2024**

Author: **Alehegn Bazezew**

Title: **Synthesizing, Characterizing and Studying Structural and Optical Properties of Pure α: PbO, Sn: α: PbO, and Co: α: PbO Prepared by Co-Pricptation Method**

Department: **Department of Physics**

Degree: **MSc.** Convocation: **Augest** Year: **2024**

Permission is herewith granted to Addis Ababa University to circulate and to have copied for non-commercial purposes, at its discretion, the above title upon the request of individuals or institutions.

Signature of Author

Dedicated to

To my family members for their limitless support, and encouragement

Acknolwledgment

Above all, I thank you to the merciful and almighty God for all he has done in my life that would have been impossible and made me being alive

Secondly my deepest gratitude goes to my advisor Prof. Fekadu Gashaw for his critical comments, constructive suggestion's and advises. Beside I would like to thank you my wife wubristgetaneh, my best friend TakeleKebede, Lemma Trife and my parents for their encouragement and motivation while conducting the study. Like Wise I am happy to thank you my friend's mitikutesfa, WuduTechane and AddisuAyalew for sharing ideas, financial and moral support to successively accomplish my study.

Finally, I would like to express my deepest appreciation and love to my parents, brother and sister for their infinite love and support. Simply, there are no words to express my undying admiration.

Lastly I would like to say thank you Addis Ababa University for helping me financially.

Table of Contents

List of figures

List of tables

List of Abbreviation

Co	cobalt
Co: α-pbo	cobalt doped alpha lead oxide
CPT	co-precipitation techniques
EDX/EDS	energy dispersive x-ray
Eg	energy gap
eV	electron volt
FTIR	Fourier Transform Infrared spectroscopy
Hr	hours
M	molar
ML	mililitres
Mn	manganese
MOCVD	metal oxide chemical vaporization deposition
MONPs	metal oxide nanoparticles
NaoH	sodium hydro oxide
Ni	nikel
NPs	nano particles
O	oxides
Pb	lead
PL	photoluminescence
Sb	antimony
SEM	scanning electron microscopy
Sn	tin
Sn: α-PbO	tin doped alpha lead oxide
SPT	spray pyrolysis techniques
TEM	transmission electron microscopy
UV-Vis	ultra violet –visible
XRD	x-ray diffraction
α-PbO	alpha lead oxide

Absrtract

In this study, undoped α-PbO and α-PbO nanoparticles doped with tin (Sn) and cobalt (Co) were synthesized using a co-precipitation technique. Characterization through XRD confirmed that the nanoparticles had a tetragonal α-PbO crystal structure, with average crystalline sizes ranging from 12.18 nm to 41.33 nm for Co and Sn doping. Reflectance spectroscopy showed that pure PbO had higher reflectance compared to Sn:α-PbO and Co:α-PbO. The optical band gaps were 1.86 eV for α-PbO, 2.86 eV for Sn:α-PbO, and 1.46 eV for Co:α-PbO, indicating a decrease in band gap with Co doping due to defect levels introduced by Co and Pb ions. Sn:α-PbO had a larger band gap than both pure PbO and Co:α-PbO. Photoluminescence studies showed lower emission for doped nanoparticles, indicating reduced electron-hole recombination. SEM revealed an average nanoparticle diameter of 5.50 nm for α-PbO, increasing to 7.8 nm with Sn doping. EDX analysis showed atomic percentages of Sn:α-PbO and Co:α-PbO as 0.63:55.15:44.22, respectively.

Keywords: pure Lead oxide tin, cobalt doping thin film, co-precipitation method, structural optical properties, XRD, PL, EDX, UV-vis, and SEM

CHAPTER ONE

1. Introduction

The term "metal oxide" describes a binary compound made up of two metal chemical elements: oxygen and another. With their wide range of technological applications, semiconducting oxide nanoparticles (NPs) and metal chalcogenide nanoparticles have attracted a lot of attention [1–5]. These applications include photovoltaic devices, lasers, light emitting diodes, liquid crystal displays, touch screens, and pseudo capacitors. Prior research has reported the fabrication of iron (Fe)-doped In2O3 nanostructures by freeze-drying and the characterization of a metal oxide material [6]. Due to its long history of employment as a photoactive layer in Schottky type photovoltaic devices, lead oxide [PbO] is one of the semiconducting oxide nanoparticles that has caught our attention [7].

Two varieties of nanostructured PbO are recognized, each with distinct opTtical and structural properties. With a band gap of 1.9 eV, α-PbO finds extensive application in photovoltaic settings [8], while PbO, possessing a band gap of 2.8 eV, is utilized as surface modifiers [9]. Lead oxide exhibits intriguing semiconducting and photoconducting qualities, making it a desirable material for use in lasers and imaging systems. PbO nanostructures in particular have drawn a lot of attention because of the material's growing interest in basic, experimental, and practical applications. Gas sensors and lead salt devices are coated with lead oxide nanoparticles for protection [10, 11, 12]. Lithium secondary batteries have also employed lead monoxide nanoparticles as an anodic material [12, 13].

Recently, there has been growing interest in the investigation and development of inorganic binary and ternary metal oxide compounds for use in optoelectronic devices. Examples include SnO [1 4], In_2O_3 [1 5], and CuO [1 6]. These materials are advantageous due to their low-cost synthesis, non-toxic nature, and environmental friendliness. In nanoparticle technology, layered or multilayered atomic structures are created with thicknesses ranging from nanometers to micrometers. This approach is significant for material synthesis, often involving wide band gap values. The properties of binary and ternary transition metal oxide nanoparticles with wide band gaps can vary greatly depending on the preparation conditions. For example, their conductivity can range from insulating to conducting [17]. Additionally, their optical and electronic properties can be enhanced for various applications such as photoconductive cells [18], electroluminescence [19], gas sensors, dielectric layers [20], and photocatalysis [21].

The advancement of nanoparticle technology focuses on the ability to control the epitaxial growth of nanoparticles on substrates and to adjust the geometric composition and structure of devices for practical applications. Among transition metal oxide nanoparticles, lead oxide (PbO) stands out due to its diverse

optical and electronic properties. PbO is well-known for its use as a photoactive layer in Schottky-type photovoltaic devices and as a modified surface layer in inverted polymer solar cells [22]. Additionally, PbO is useful in heating applications for homes in temperate regions and in agriculture [23].

PbO is crucial in forming the active electrode mass in lead-acid batteries, which are valued for their high power density, wide temperature tolerance, complete recyclability, and relatively low cost [24]. Lead, with oxidation states of +2 or +4, leads to various forms of PbO nanoparticles, making it challenging to deposit them in a single, well-defined crystal phase [25]. Lead oxide exists in several forms, including PbO, $Pb2O_3$, Pb_3O_4, PbO_2, and polymorphic phases such as α-PbO and β-PbO [26]. These different phases result in varying reflectance levels in laser writing, making PbO suitable for multi-valued logic optical storage devices and gas sensors [27, 28]. The synthesis of PbO nanoparticles can be difficult due to their high volatility at relatively low temperatures [29]. Techniques for depositing PbO include metal-organic chemical vapor deposition (MOCVD) [30], sputtering [31], electrodeposition [32], and co-precipitation. Among these, co-precipitation is particularly attractive due to its low temperature processing, which allows precise control over nanomaterial properties. It is also noted for being simple, cost-effective, and reliable compared to other synthesis methods.

UV-Vis spectroscopy was used to investigate the reflectance, absorption, and energy band gap of PbO nanoparticles. By adjusting the preparation method, temperature, and dopant concentration, the properties of these nanoparticles such as energy gap, crystallinity, and photoconductivity can be fine-tuned [33-37]. Research has increasingly focused on the effects of doping on PbO nanoparticles, revealing that the insertion of nickel ions significantly reduces crystallite size [38, 39]. Zn-doped PbO nanoparticles, for example, exhibit well-defined crystallinity and altered optical properties depending on the Zn concentration [40]. It has been previously reported [41-44] that elements from the 3d series, such as Mn, Co, Fe, Ni, and Zn, serve as excellent precursors for synthesizing pure and homogeneous oxide nanoparticles with high surface areas due to their low decomposition temperatures. Among these 3d elements, Mn doping in metal oxide semiconductors is particularly notable for enhancing optical properties, making them suitable for solar cell applications [42-49]. Mn-doped ZnO and CdO nanoparticles prepared via spray pyrolysis have demonstrated that Mn doping can effectively tune the band gap [42-47]. Specifically, for Mn-doped ZnO thin films, the optical band gap increases with higher Mn concentrations, while for CdO films, both the crystallite size and optical band gap decrease with increased Mn doping. Similarly, PbO nanoparticles show promise as materials for solar cells, particularly for use as windows and buffer layers, due to their favorable properties transparency in the visible region.

Based on earlier studies, it is expected that doping of Mn allow to tune the optical properties of PbO nanopaticles.

The aim of this work is to evaluate the effect of Sn and Co doping on the structural and optical properties of α-PbO nanoparticles grown by co-preciptation method. It may also be noted here that a systematic investigation to understand the optical and stractural properties of the Sn and Co doped α-PbO nanoparticles has not yet been performed. This study will give support to the preparation of other metal doped pure alpha lead oxide nanostructured nanoparticles for optical applications. The structural, morphological and optical properties of synthesized α-PbO and Sn , Co doped α-PbO nanoparticles has been investigated by using XRD, SEM analysis and UV-Visible spectroscopy.100037819245

1.1 Metal oxide nanoparticles

Metal oxides are crucial in various fields such as chemistry, physics, and materials science [50, 51]. The metal elements are able to form a large diversity of oxide compound [52 Metal oxides can adopt a wide range of structural geometries and exhibit various electronic properties, such as metallic, semiconductor, or insulating behavior. In technology, they are utilized in creating microelectronic circuits, sensors, piezoelectric devices, fuel cells, protective coatings against corrosion, and catalysts. Oxide nanoparticles, due to their small size and high density of surface sites, can display unique physical and chemical properties. The size of these particles is anticipated to impact three key sets of fundamental properties, starting with structural characteristics, including lattice symmetry and cell parameters [53]. This structural phenomenon has been detected in TiO_2, VOx, and Al_2O_3 oxides [54, 55, and 56]. Size-induced structural distortions associated with changes in cell parameters have been observed, for example, in nanoparticles of Al_2O_3 [55] ,NiO[57], Fe_2O_3[58] ,ZrO[59] ,MoO_3[61], CeO_2[60] and Y_2O_3[61]. As the particle size decreases, the increasing number of surface and interface atoms generates stress/strain. Stress/strain is produced by the growing number of surface and contact atoms as the particle size reduces. The oxide's electrical characteristics are the subject of the second significant effect of size. The so-called quantum size or confinement effects are produced by the nanostructure in any material and are primarily caused by the existence of discrete, atom-like electronic states. In a simplistic classification, the third set of properties influenced by size is the physical and chemical properties of the solid, which are clearly driven by its structural and electrical properties.

A decrease in the average size of an oxide particle do in fact change the magnitude of the band gap[62,63] with strong influence in the conductivity and chemical reactivity[64,65]. Furthermore, we will provide a brief overview of the limited research conducted on various single oxide systems that

comprise Zn, Fe, and Sn. Despite the publication of a recent review on the catalytic utilization of solid solutions, far less is known about nanostructured mixed oxides.

1. - Aluminium oxides. The Al-O system focuses primarily on Al2O3 due to its significant role as a catalyst, absorbent, and ceramic material in various industrial applications. Recent advancements involve using novel nanostructured aluminas as supports for active catalytic phases or coating them with materials such as YAG or nano-Ni/-W. These coatings enhance the mechanical properties of the aluminas, providing exceptional resistance to deformation at moderate temperatures (Ni, W)[66,67].

2. - MgO and other alkaline-earth oxides. Magnesium oxide (MgO) is widely used in the chemical industry as a scrubber for air pollutant gases (CO2, NOx, SOx) and as a catalyst support [68]. It exhibits a rock salt structure like oxides of other alkaline earth metals. The non-polar (100) face is by far the most stable surface [69, 70, 71] and particles of MgO usually display a cubic shape. For example, when Mg metal is burned in air or oxygen, the MgO smoke particles that are formed are almost perfect cubes having (100) faces [72] Special procedures to prepare MgO nanoparticles exhibiting (110) and (111) faces have been partially successful [73] but in general they tend to facet to surfaces containing (100) plane [74]. The rock salt (110) surface is also non-polar, but its surface energy is twice that of a (100) surface. In the case of a (111) surface, the situation is more complex because it will contain either a layer of Mg cations or a layer of O anions. Neither of these planes is charge neutral (a net dipole moment exists). Thus, MgO nanoparticles exhibiting (111) faces are intrinsically unstable and should undergo a structural transformation.

1.2 Doped metal oxide nanoparticles

Doping is a clear method to alter the phase transformations discussed by initially occupying some interstitial sites within the polymorphs. This process changes the paths of cation movement and causes the dopants to increasingly accumulate at the surface layer of the material's grain boundaries as the temperature rises.

Ce-containing mixed-metal oxides. The performance of ceria in automotive catalysts and fuel cells can be enhanced by doping this oxide with a second metal (M= Zr, Ca, Cu, Au, Pt, Tb, La, Mn, etc) [77, 78 79]. Mixed-oxides maintain fluorite-type structures, particularly the cation sub-lattice, up to a high level of doping. The doping element in many cases enhances the thermal stability of the support system or favors the transport of oxygen (conversion between "Ce^{3+}" and "Ce^{4+}" oxidation states). In some situations, the doped-ceria nanoparticles become very active catalysts for reactions such as the water-gas shift or the destruction of SO_2 [75, 76]. This effect is achieved by doping with noble metals like Cu, Au

or Pt, and the phenomenon is not fully understood [80, 81 82]. However, as described below, these properties of ceria-based systems are mainly driven by two physico-chemical phenomena; the local M-O ordering and distance and the way the systems achieve charge neutrality, which in the case of ceria is mainly through presence of oxygen vacancies

1.3 Application of metal oxide nanoparticles (MONPs)

Transparent conducting oxides (TCOs) such as indium oxide, tin oxide, zinc oxide, and cadmium oxide have diverse applications in optoelectronic devices. Among these, cadmium oxide (CdO) is particularly notable for its use in gas sensors, photovoltaic photodiodes, and transparent electrodes, owing to its low resistivity, high carrier concentration, and excellent optical transmittance in the visible spectrum [83, 84]. Despite its acute toxicity through oral, dermal, and inhalation exposure, CdO is employed because of its unique properties and applications. Lead oxide is a crucial semiconductor with significant applications in storage batteries, the glass industry, and pigments [85]. It exists in various forms, including PbO (α, β, and amorphous), Pb2O3, Pb3O4, and PbO2 (α, β, and amorphous). Its unique electronic, mechanical, and optical properties make it valuable in industry, with potential uses in nano-devices and functionalized materials [86]. PbO comes in two main forms: yellow β-PbO, which is stable at high temperatures, and red α-PbO, which is stable at lower temperatures. The transition from α-PbO to β-PbO occurs at approximately 490 °C [87]. Furthermore, lead oxide serves as an important glass modifier, enhancing the thermal, optical, chemical, and mechanical stability of glass.

1.4. General properties of alpha lead oxide

Lead (II) oxide, also known as red lead oxide, is a powder with an orange or red hue. It is a water-insoluble substance that is made when metallic lead or litharge (lead monoxide) is oxidized. These materials size, shape, and physical, chemical, electrical, and optical characteristics are all dependent on each other, and their bulk properties frequently differ significantly. Lead oxides have strong absorption cross section area, high carrier mobility, and high conductivity.

1.4.1 Physical properties

. The alpha form constitutes tetragonal crystals, while the beta modification is a yellow amorphous powder of orthorhombic crystal structure. The alpha form is stable at ordinary temperatures, converting to the beta form when heated at 489 ^{0}C; density 9.35 g/cm^3 (beta form); Moh's hardness 2 (alpha form); the oxide melts at 888 ^{0}C; vaporizes at 1,472 ^{0}C with decomposition; vapor pressure 1 torr at 943 ^{0}C and 5 torr at 1,039 ^{0}C; practically insoluble in water (the solubility of alpha form is 17 mg/L at 20 ^{0}C and that of beta form 23 mg/L at 22 ^{0}C); insoluble in ethanol; soluble in dilute nitric acid and alkalies.

1.5 Statement of the problem

Synthesizing and characterizing of the structural and optical properties of pure α-PbO, Sn: α-PbO and Co: α-PbO has been the subject of great deal of research/thesis. A study explored the effective and efficient targeting of finding precursors & how we can synthesize, characterize and study the structural and optical properties of pure alpha lead oxide & how do we dope tin and cobalt to pure lead oxide.

1.6 objective

1.6.1 General objective

The objective of this thesis is to synthesize, characterize, and study the optical and structural properties of cobalt and tin doped on pure α: PbO, which is made using the co-precipitation method.

1.6.2 Specific objective

The specific objectives of this thesis include the following

- ✓ To synthesize Pure α: PbO, Sn: α: PbO, and Co: α: PbO nanoparticles utilizing the co-precipitation method.
- ✓ To characterize the crystal structure of Pure α: PbO, Sn: α: PbO, and Co: α: PbO nanoparticles using techniques such as X-ray diffraction (XRD).
- ✓ To analyze the morphology and particle size of the synthesized nanoparticles through scanning electron microscopy (SEM).
- ✓ To investigate the chemical composition and elemental mapping of the nanoparticles using energy-dispersive X-ray spectroscopy (EDS).
- ✓ To compare the structural and optical properties of Pure α: PbO, Sn: α: PbO, and Co: α: PbO nanoparticles to identify the influence of dopants on these properties.

1.7 Significance of the problems

To significantly advance our understanding of optical and structural effect of Sn and Co on pure alpha lead oxide. The co precipitation technique is used to prepare pure lead oxide and the researcher tries to show how pure lead oxide was prepared by using the technique. The method of characterization are XRD, PL, UV-vis, SEM and EDX to instigate the crystalline size or purity, structural analysis, the impurity level of a material and it also knowledge of about an estimate of interface disorder and roughness, optical properties in surface morphology and elemental analysis, respectively.

1.8 The research gap

Synthesizing and characterizing of nanoparticles by prepared co-precipitation technique were already have made by number of researchers. the researchers were performed synthesizing number of metal

oxides (binary and ternary metal oxide) but tin and Cobalt doped pure lead oxide were not performed by any other researchers or there were no any literature review on the effect of structural and optical properties of tin and cobalt doped pure alpha lead oxide. The gaps of the thesis were the structural and optical effect of tin and cobalt on pure alpha lead oxides prepared by co precipitation technique.

1.9 Scope of the thesis

Hence, it is essential to tackle the limitations associated with the synthesis, characterization, and examination of the structural and optical properties of both undoped and doped pure lead oxides. The synthesizing method used in these thesis were co precipitation techniques. A preparation process uses a materials as a precursor's as a starting material and prepares a binary nanoparticles. The as prepared nano particles were dried in an oven at 100 ^{0}C for two hours. The purpose of these studies was synthesizing binary and ternary metal oxides nanoparticles that have significant interest for the developing of optoelectronic device and applications. Additionally electrical and optical properties might enhance for variety of uses. In these researches the researcher uses different characterization technique.

CHAPTER TWO

2 Review literature

2.1 Metal oxide nanoparticle

Recently, metal oxide semiconductor nanoparticles have drawn alot of attention because of their distinctive potential for various applications .Most commonly, metal salts are hydrolyzed at room temperature or at temperatures no higher than 100 ^{0}C to produce metal oxide nanoparticles (MONPs).Thesemetaloxidenanoparticles possessanelectronicstructureand a widerange ofstructural geo metries. Same the metal oxides are SnO, ZnOand PbO.

2.1.1Tin oxide (SnO)

SnO nanoparticles were produced using a microwave-assisted hydrothermal method. It was observed that at microwave powers of 300 and 600 watts, SnO formed and remained in the tetragonal phase. However, at 900 watts, SnO2 began to appear, resulting in a mixture of SnO and SnO2 phases. The particle size ranged from 2 to 13 nm across the different power levels. UV-V absorption spectra revealed excitonic peaks at 288, 300, and 315 nm, corresponding to crystal sizes of 2, 6, and 10 nm, respectively. No excitonic peaks were detected for particles larger than 10 nm. These excitonic peaks are likely due to the transition from an indirect band gap in bulk SnO to a direct band gap in SnO nanoparticles. To confirm this, photoluminescence spectroscopy was performed, and a strong emission at 677 nm upon excitation at 336 nm supported this hypothesis [88].

2.1.2 α and β phase lead oxide (PbO)

α and β phase lead oxide (PbO) nanoparticles were synthesized using a straightforward chemical precipitation method. Characterization of the samples was performed through X-ray diffraction (XRD), UV-visible (UV-vis) spectroscopy, and photoluminescence (PL) spectroscopy. XRD results confirmed the tetragonal structure for α-PbO and the orthorhombic form for β-PbO nanocrystallites, with average crystallite sizes of 36 nm and 47 nm, respectively. UV-Vis spectra indicated direct band gap energies of 3.91 eV for α-PbO and 3.85 eV for β-PbO. PL studies showed blue and green emissions attributed to excitonic recombination and defects generated during synthesis. No near band edge emission peaks were observed. The defect density in α-PbO was found to be lower compared to β-PbO [89]

2.2 Metal doped Metal oxides

2.2.1 Zinc doped lead oxide (Zn: PbO)

Zinc (Zn)-doped lead oxide (PbO) nanoparticles were synthesized with varying Zn doping concentrations using a chemical precipitation method. X-ray diffraction analysis revealed a shift in 2θ values towards higher angles, suggesting that Zn^{2+} ions are substituting for Pb^{2+} ions in the lattice. High-resolution transmission electron microscopy and selected area electron diffraction (SAED) patterns confirmed the crystalline nature of the samples. The presence of Zn atoms introduces impurity energy levels in PbO, as indicated by the energy gap values observed in ultraviolet-visible spectroscopy. Photoluminescence spectroscopy further analyzed the defect levels in the samples. The results suggested that a 0.1 M Zn doping concentration is optimal for achieving well-defined crystallinity and altered optical properties, making it suitable for use in photoluminescent materials [89]

2.2.2 Tin doped cadium oxide (Sn: CdO)

Transparent conducting Tin-doped Cadmium oxide (CdO) thin films were fabricated using the sol–gel spin coating technique with varying Sn concentrations. X-ray diffraction analysis indicated that the CdO films are polycrystalline with a cubic structure, showing a preferential orientation along the (111) plane. Surface morphology was examined using scanning electron microscopy (SEM), and surface roughness was assessed through water contact angle measurements. Energy-dispersive X-ray spectroscopy (EDX) confirmed the presence of Cd, Sn, and O elements in the films. The observed blue shift in the energy gap from 2.42 to 2.96 eV is attributed to the Burstein–Moss effect. Functional groups and chemical bonding were verified by Fourier-transform infrared (FTIR) spectroscopy. The thin film with 5% Sn doping exhibited the lowest electrical resistivity (1.12×10^{-4} Ω·cm) and the highest carrier concentration (9.94×10^{21} cm^{-3}) [90] .

2.2.2 Copper doped Zinc oxide (Cu: Zno)

The impact of copper doping on the structural, electrical, and optical properties of zinc oxide (ZnO) nanoparticles was investigated. Copper-doped ZnO nanoparticles (ZnO: Cu) were successfully deposited onto glass substrates via spray pyrolysis, with doping levels of 0, 2.5, and 7.5 at% (ZnO, ZC2.5, ZC7.5). All nanoparticles were found to be polycrystalline and single-phase, maintaining the hexagonal wurtzite structure of ZnO. The films exhibited nanostructured crystallites ranging from 36.7 to 38.2 nm. Copper

doping enhanced the electrical conductivity of the ZnO nanoparticles, with conductivity improvements directly proportional to the Cu concentration. The nanoparticles showed high optical transmittance of 70-80% in the visible spectrum. Copper doping led to a reduction in the energy gap. Photoluminescence spectra revealed strong ultraviolet emissions and weaker blue emissions, with the emission wavelengths shifting to lower values as the dopant concentration increased. The ZC7.5 sample demonstrated the most favorable characteristics for use as a transparent conducting oxide, featuring intense optical transmittance, strong UV photoluminescence, and the lowest electrical resistivity [91].

CHAPTER THREE

3 Materials and Method

3.1. Material

The materials used in the experiment are beaker, magnetic stirrer, centrifuge, distilled water, ethanol, dropper and drying oven and precursors used in the experiments are tin dichloride, cobalt acetate, lead acetate and sodium hydroxide

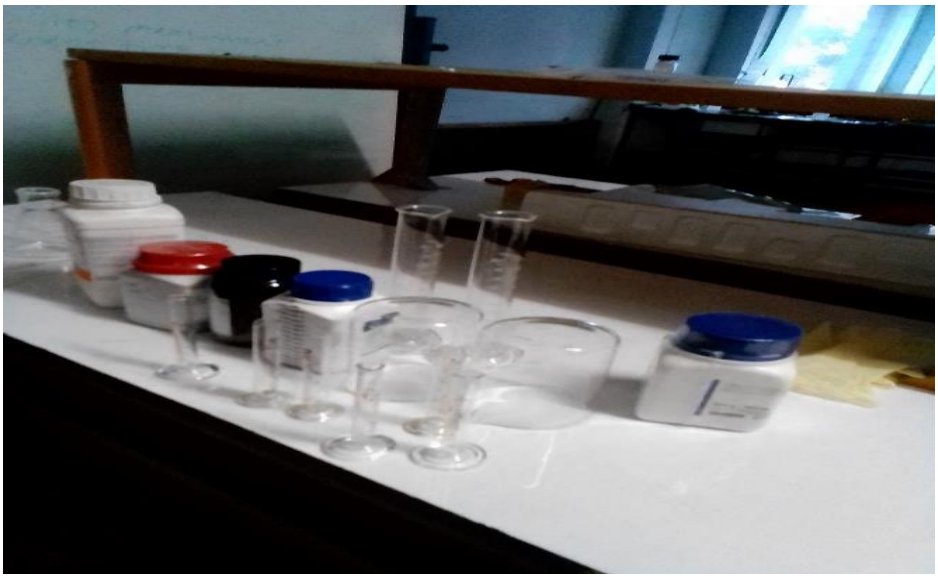

Figure 1 material used in synthesis of pure α-pbo and Sn, Co doped with pure α-pbo

3.2 Experimental procedures

One mole of lead acetate dissolved in 100 ml of distilled water. The solution was stirred continuously by magnetic stirrer until it becomes clear solution. 19 M of NaOH was added in to 100 ml of distilled water is used as a reducing agent, this 40 ml of NaOH solution was added to lead acetate solution in a drop wise. The rxn temperature was fixed to 85 ^{0}C under a string.as the solution was added initially changed to milky like color .after continuous adding of NaOH solution in drop wise the solution becomes cloudy and then changed to deep color after two hrs the precipitation was filtered and then was washed by distilled water and ethanol, then drying in hot air oven at 100 ^{0}C for an hr.

The colour change during the synthesizing or preparation show as there is nucleation or there is reaction and this reaction brings the colour change.

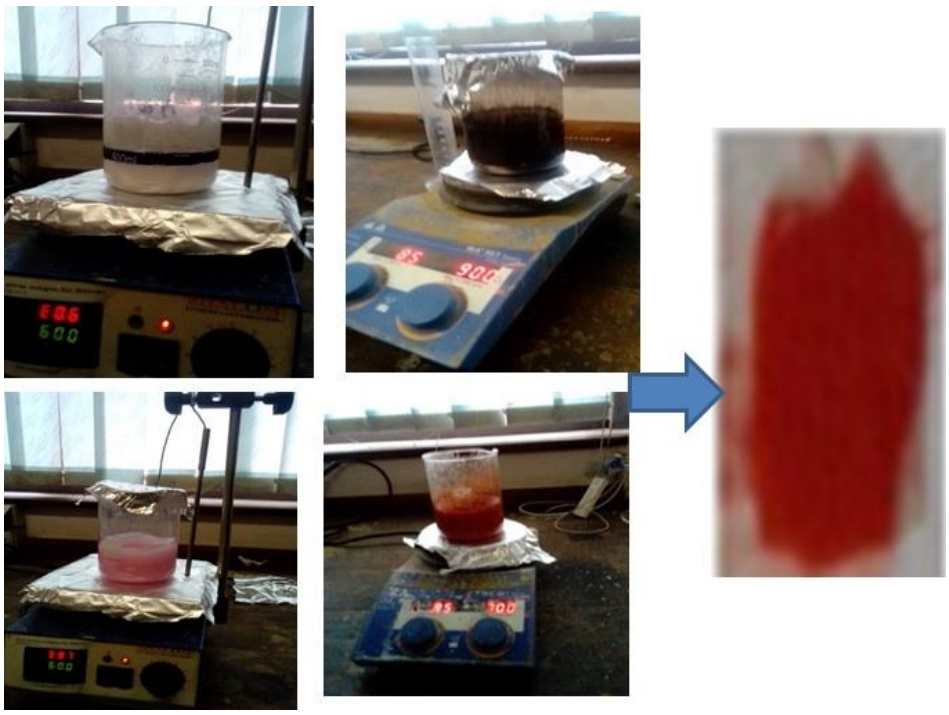

Figure 2 procedure used in the synthesis of pure α-pbo and Sn, Co doped with pure α-pbo

3.3 Nanoparticles deposition techniques

Several methods have been used to synthesize or deposit thin films or NPs. These include physical vapor deposition, sol-gel deposition technique , spray pyrolysis technique (SPT) , electron beam evaporation deposition, reactive magnetron sputtering, pulsed laser deposition , chemical vapor deposition (CVD), chemical bath deposition or chemical solution method and co-precipitation technique Among these technique chemical Co-precipitation techniques are a simple ,economic and industrial techniques that can be used for the synthesis of important metal oxides nanoparticles or materials, such as pure lead oxide tin doped pure lead oxide and cobalt doped pure lead oxide

3.3.1 Co-precipitation techniques

Co-precipitation technique is the term used to describe the precipitate being contaminated by substances that are typically soluble in the mother liquor.In co-precipitation; a metallo-organic precursor goes through nucleation, followed by aggregation or Ostwald ripening to form metal oxides. This is a step-by-step chemical synthesis of nanoparticles. The size of the metallic oxide nanoparticles is regulated by secondary processes, specifically Ostwald ripening.

When an impurity's ionic radius and charge are similar to those of the carrier, it may occupy a lattice site in the carrier's crystal structure, resulting in a crystallographic defect known as an inclusion.

An adsorbat is an impurity that is only loosely adhered (adsorbed) to the precipitate's surface. When an adsorbate impurity becomes physically trapped inside the crystal as it develops, it results in an occlusion. Co-precipitation techniques can be reduced by using a diluted and pure solution, double precipitation, aging or digestion processes, organic solvent use, slow reagent addition, stirring, and the right temperature.Itseactions occur when nucleation,growth, coarsening, and/or agglomeration processes take place all at once. The following traits of co-precipitation reactions are seen in their products: A large number of small particles will be formed during the critical step of nucleation, which is important; a significant impact is made on the size, morphology, and properties of the products by secondary processes like aggregation. Usually, a chemical reaction produces the super saturation conditions requiredtocause precipitation .The following are common co-precipitation synthetic techniques: oxides formed from aqueous and non-aqueous solutions; metals formed from aqueous solutions by reduction from non-aqueous solutions; and electrochemical reduction and decomposition of metal organic precursors.Microwave/sonication-assistedco-precipitation producesmetalchalconides.

Depending on the precipitating agent chosen for the reaction, this method has the advantage of producing crystalline sizes in the small range when compared to other synthesis processes.The coprecipitation method hasthefollowingbenefitslowtemperature, energy efficient, easy control over the particle size and composition easy preparation, quick and easy modification of the particle surface state and overall homogeneity, and no need for the use of organic solvents. Drawbacks include not applicable to species that are not charged; trace impurities may precipitate with the product; and issues with reproducibility from batch to batch. If the reactants precipitate at signifoicantly different rates, this method is not effective**.**

3.3.2. Factors effecting co-precipitation techniques

Temperature, dosage rate, centrifuging, and stirring speed are a few of the variables that can affect CPT. When strong acid is added, a salt of strong acid that is only weakly soluble becomes more soluble. Strong acid addition lowers the activity coefficients of both ions of the sparingly soluble salt by raising the ionic strength of the solution. The effect of temperature on a precipitate's solubility is that it becomes more soluble as the temperature rises. A solute dissolves primarily through endothermic reactions, so as the temperature rises; the solubility product constant does as well. The nature of a solvent has a significant impact on a solute's solubility. This is evident in the precipitate's solubility. Polar solutes tend to dissolve more readily in polar solvents, while nonpolar solutes tend to dissolve more readily in nonpolar solvents. Water that has an organic solvent added to it becomes less soluble in inorganic compounds. A

substance's solubility increases with decreasing particle size, leading to super saturation and precipitate formation. Any solution with more solute in it thean would be expected under equilibrium conditions at a particular temperature is said to be supersaturated. The precipitate's particle size is significantly influenced by super saturation.an increase in reactant concentration, the precipitate's particle size decreases.

3.3.3 Nanoparticle characterization techniques

3.3.3.1 XRD

X-ray diffraction (XRD) is one analytical technique that is widely used to determine the dimensions of unit cells and identify crystalline materials. Every substance generates a different X-ray signature. The X-ray pattern displays the characteristic of its crystalline atomic structure: X-ray intensity versus scattering angle. Comparing an unknown material's XRD pattern to a library of known patterns allows for qualitative analysis. Consequently, it is one of the most effective methods for both the qualitative and quantitative analysis of crystalline compounds. The method provides information on the kinds and characteristics of phases that are present, the structural composition of phases, the degree of crystallinity, the amount of amorphous content, micro strain, the size and orientation of crystallites, and more. X-rays that are incident upon a crystal are scattered in various ways. Every substance generates a different X-ray signature. A set of well-defined beams arranged with a characteristic geometry form a diffraction pattern when the scattering, also known as diffraction, occurs when the wavelength of the radiation (λ) is comparable to the atomic spacing in a crystal.The X-ray pattern displays the X-ray intensity versus scattering angle that is characteristic of its crystalline atomic structure. Diffraction data collection is the outcome of relative intensity (I) and corresponding scattering angle (2theta) measurements for each reflection with a set of crystal planes identified by Miller indices (h k l), The positions and intensities of the diffracted beams depend on how the atoms are arranged in space as well as some other atomic characteristics. The arrangement of the atoms in the crystal and their chemical makeup can therefore be inferred from the positions and intensities of the diffracted beams, which are also known as reflections, spots, or lines. Only if the geometry of the situation satisfies a very specific law defined by Bragg, known as Bragg's law, will a beam of radiation be diffracted when it is imposed upon a set of planes in a crystal.

$$n\lambda = 2d_{hkl}\sin\theta \qquad (1)$$

The equation (1) is called the Bragg equation; n stands for the order of diffraction, λ is for wavelength, d is the inter planar spacing of the h, k, l planes in the crystal lattice, and θ is for Bragg angle [1].

Application of XRD include crystal phase identification, lattice constant determination, phase purity determination, investigation of phase changes, refinement of structure, and crystallite size determination.

3.1.3.2 UV-Vis spectroscopy

The three phenomena of transmission, reflection, and absorption are used to examine the optical behaviors of semiconductors. When light shines on a semiconductor, photons strike the surface, some of which are reflected, some of which are absorbed by the semi conductor, and the remainder of which are transmitted into the semiconductor, some of which may be reflected. Here to calculate optical band gap of nanoparticles and then other optical parameters from observation of transmission and absorption property of prepared samples by Ultraviolet-visible spectroscopy meter. In the ultraviolet-visible spectral range, absorption spectroscopy or reflectance spectroscopy are referred to as ultraviolet-visible spectrophotometers (UV-Vis or UV/Vis). This indicates that it makes use of light that is visible, and near-UV and near-infrared (NIR) in wavelength. The visible absorption or reflectance of the chemicals involved directly affects how those colors are perceived. Molecules go through electronic transitions in this area of the electromagnetic spectrum. Fluorescence spectroscopy deals with transitions from the excited state to the ground state, whereas absorption measures transitions from the ground state to the excited state, making it a complementary technique to fluorescence spectroscopy. The Kubelka-Munk function is used to determine reflectance.

$$F(R) = (1-R)^2/2R \qquad (2)$$

Where F(R) is known as kubelka–munk function and R is the reflection of the materials. The following data are obtained from UV-vis spectroscopy: absorbance, transmittance, band gap energy, and reflectance

3.3.3.3 Photoluminescence (PL)

A molecule absorbs a photon in the visible spectrum that excites one of its electrons to a higher electronic excited state and then emits a photon as the electron returns to a lower energy state. This process is known as photoluminescence. It is a method of material probing that is non-contact and non-destructive. In essence, light is shone onto the sample, which absorbs it and allows for the possibility of a process known as photo-excitation. The photo-excitation causes the material to jump to a higher electronic state, and will then release energy, (photons) as it relaxes and returns to back to a lower energy level. The primary work or information obtained from photoluminescence is as follows: Determination of Band Gap: In semiconductors that display radiative transitions, the band gap is the energy difference between the valence band (bottom) and the conduction band (top). A semiconductor's PL spectrum range is used for non-destructive band gap analysis. Using this mode, one

can quantify the elements that make up a semiconductor compound as well as the material specifications that are vitally important for influencing the performance of devices like solar cells. Defect and Impurity Level Identification: When a radiative transition happens in semiconductors, certain localized defect levels are produced. The photoluminescence energy can identify specific defects associated with these levels, while the amount of photoluminescence (PL) can determine their concentration.

Low-temperature photoluminescence spectra of the sample frequently show peaks in the spectra linked with the impurities present in the host material. Highly sensitive Fourier transform photoluminescence has the potential to detect very low concentrations of intentional and un intentional impurities, which have a significant impact on both the performance of the device and the quality of the material. Recombination phenomena the "recombination" (return to equilibrium) mechanism are used in both radiation-based and non-radiation-based processes.

The relative quantity of radiative and nonradiative recombination rates is directly correlated with the amount of PL that a material emits.

Particular defects related to these levels can be recognized by the photoluminescence energy whereas their concentration can be ascertained by the PL amount. Hence, qualitative PL analysis includes the monitoring of the change in material quality as a function of some conditions like growth as well as processing, which helps in understanding the fundamental physics of the recombination mechanism. Some widely used conventional techniques, such as XRD, and Raman spectroscopy, are frequently in sensitive to surface structure and excited states for catalysts that are oxide supported with low metal oxide concentrations. However, PL is overly susceptible to surface effects and semiconductor-based particles.

3.3.3.4 EDX (energy dispersive x-ray)

Edx/eds/edsa is characterization technique used to determine the composition of the sample; it's effective for major and minor elemental analysis and identifies the elemental analysis. An electron beam is used to excite the atoms in a sample using a scanning electron microscope (SEM) fitted with an x-ray detector. When this beam interacts with the atom, an electron is forced out of its shell and a void is left behind. This hole in the lower orbital is filled by another electron that is of a higher energy level. The amount of energy released during this process depends on how many shells, the replacement electron has moved and which shell it has moved from its initial position. The detector transforms the x-rays that are released by this energy into voltage. Counts that represent the quantity of x-rays at each energy level make up the final data. The energy level of the x-rays that are released is related to specific elements, and the

proportional counts are related to the amount of the element. The data that EDX provides us with is as follows: it is utilized for chemical composition analysis to identify and quantify elemental composition in very small quantities of materials. It identifies the presence of pb and o in pbo Nano materials as the dominant elements. Use all available techniques for quantitative and qualitative analysis of the relative concentration of elements.

3.3.3.5 Scanning electron microscopy (SEM)

Scanning electron microscopy or SEM produces detailed, magnified images of an object by scanning its surface to create high resolution images .The resulting image shows information about what the object is made of and its physical features .the instrument which obtain this information about composition and topography is scanning electron microscope .The instrument used for this includes electron source , anode , condenser , scanning oil , and objective lens .The two types of electrons essential for imaging are backscattered electron and secondary electron .Back scattered electrons are reflected back when the primary electron beam interact with the sample object .these are elastic interaction .secondary electrons are different because they come from atoms of the sample and are the result of in elastic interaction. SEM image provide information on topography, composition and morphology .topography is the distribution of features or parts on the surface of sample. Composition what sample is made of and morphology is the form shape or structure of the sample. The scanning electron microscope (SEM) is the most widely used type of electron microscope. It examines microscopic structure by scanning the surface of materials, similar to scanning confocal microscopes but with much higher resolution and much greater depth of field. In comparison to the wavelength of light (5×10^{-7} m), electrons have much shorter wavelengths of between 1×10^{-11} m to 1×10^{-12} m with respect to the accelerating voltage applied, which allows for better resolution up to 1 nm in an electron microscope than that of conventional optical.

CHAPTER FOUR

4. Result and Discussion

4.1 X-ray diffraction (XRD) ananlysis

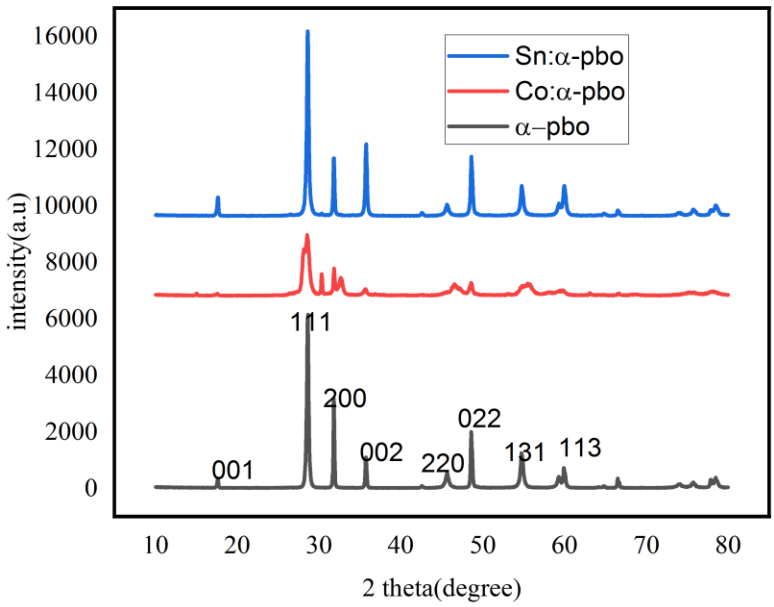

Figure 3 the XRD intensity of α-PbO, Co: α-PbOand Sn α-PbO

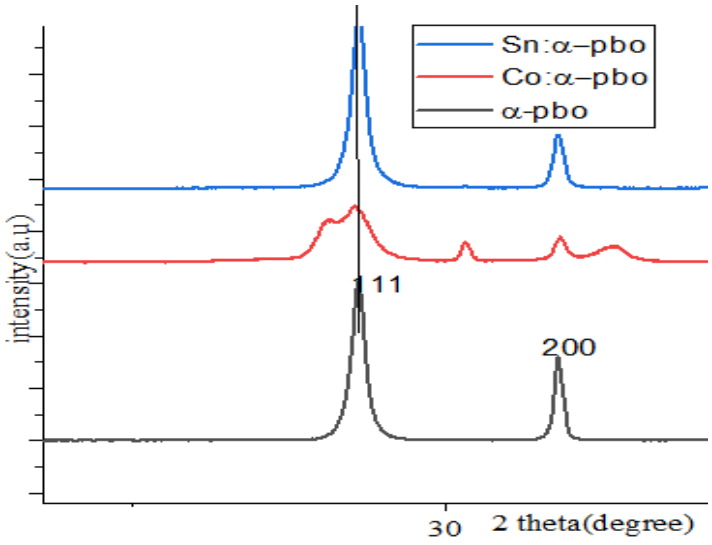

Figure 4 the expanded version of of α-PbO,Co: α-PbOand Sn:α-PbO

Pure α-PbO and Sn, Co doped α-PbO nanoparticles were deposited on the glass substrate using co-precipitation technique were characterized by XRD that is to determine crystallite size, crystalline stracture, determination of lattice constant and determination of unit cell volume.

Figure 3 shows the XRD patterns of un-doped α-PbO and Co, Sn doped α-PbO Nano particle samples. It is revealed from the X-ray diffraction pattern of the samples that all diffraction peaks (>10°) could be assigned to the tetrahedral phase of α-PbO (JCPDS file no. 005-561). The diffraction peaks around angles of 17.5^{o} , 28.63°, 31.83°, 35.746°,45.61^{0} 48.62°,54.74° and 59.94^{o} are clearly detected, which, respectively, correspond to the (001), (111), (200), (002), (220) , (022), (131) and (113) Miller planes of the α-PbO. The appearance of sharp and number of diffraction peaks reveals the polycrystalline nature of the nanoparticle. The XRD result confirmed that the prepared samples had a tetragonal crystal structure with lattices parameter a = b = 5.951 Å & c = 8.266 Å and α = β =& γ = 90^{0}. As demonstrated in the figure 3 the intensity of Sn: α-PbO nanoparticles increases in the plane (111) when compared to pure α-pbo and this is due to the fact that Sn improves the development rate/enhances crystallinity of pure α-PbO nanoparticles, the d- spacing decreases or the crystalline compress and gives the higher degree of crstallinity than pure α-PbO and Co: α-PbO nanoparticles resulting in sharp diffraction peak in the XRD. The intensity of Co doped α-PbO nanoparticles is lower than that of pure α-PbO and Sn doped α-PbO nanoparticles.This is because of cobalt deteriorates the the crystallinity of the pure alpha lead oxide and Sn/Co the orientation of the pure α-PbO . It is interesting to note that for undoped α-PbO, the intense peak is at 2θ = 28.630 (111) plane, there were a shift in intensity of peak for doped samples.This shift to the lower angle for Co doped α-PbO indicates that the lattice parametrs are varied than pure α-PbO and successful incorporation Co^{2+} in to the host lattice. The reduction in peak intensity is because of declination of the crystallinity and the incorporation of cobalt atom in the pure α-PbO nanoparticles.This shift towards the lower angle and the broadening of Co: α-PbO is the result of declination of the crystallinity quality and associated to the lattice distortion, the increase of d-spacing and the strain induced in α-PbO lattice due to mismatch of Co and pb ions .The same result werereported for Mn: PbO [92].

.Diffraction with Sn can be perfectly indexed to α-pbo according to peak position of (JCPDS 05 05 61) and no impurity peak was observed, which indicates that obtained product was pure α-PbO. The XRD pattern of obtained α-pbo structure and Sn: α-pbo and compounds from the figures α-PbO no characteristics peaks, such as α-pbo were observed, indicating high purity products. The absence of any peak from Sn: α-pbo confirms that Sn act as substitutional dopant. The substitution of Sn in Pb cause a decrease in the lattice constant and the crystallite size due to different size of ionic radii .The ionic radii of tin 0.67 and Pb is 1.19Å. Of cobalt is 0.74 Å and the ionic radius of lead is 1.19 Å.

Diffraction with Co can be perfectly indexed to α-PbO according to peak position of (JCPDS 05 05 61) and no impurity peak was observed, which indicates that obtained product was pure α-PbO. The XRD

pattern of obtained α-PbO structure and Co: α-PbO compounds from the figures 3 α-PbO no characteristics peak, such as α-PbO were observed, indicating high purity products. The absence of any peak from Co: α-PbO confirms that Co act as substitutional dopant. The incorporation of Co into Pb results in a reduction of the lattice constant, peak intensity, and crystallite size, which can be attributed to the variation in ionic radii. The crystalline size for the prepared NPs was analyzed from three most prominent diffraction peak of (001), (002) & (200) plane using Debey Scherer relation shown in equation (3)

$$D = K\lambda/\beta COS\ \theta \ldots\ldots\ldots\ldots\ldots\ldots\ldots\ldots (3)$$

where D is average crystal size obtained from the two dominant peak ,K is constant for shape factor nearly equal to 0.9, λ is the wave length of x-ray used (Cu Kα, λ= 0.15406 nm) β is full width at half maximum and θ is the angle of diffraction of three peak.

The average crystalline was calculated from the of miller index peak of α-PbO to (001) (002) & (200) and would be 41.329 nm for α-PbO 12.176nm for 2% Co: α-PbO & 32.822 nm for 2% Sn: α-PbO. Further the crystalline size were decreased from 41.329nm to 12.176nm.

The D value of Co: α-PbO from 41.329 nm to 12.176 nm this revels that the incorporation of Co ion into Pb and leads to the deterioration of crystalline quality of Co: α-PbO and increasing the grain baoundaryin α-PbO.

The expanded version of XRD (figure 3) clearly shows the slight position shift at(111) Co: α-PbO shifts to the lower difraction angle when compaire to pure α-PbO NPs . This peak shift to the lower angle for doped NPs indicates that the lattice parameter are varied than the pure α-PbO and successful incorporation of Co and Sn.

From the XRD peak the lattice parameters for the tetragonal crystal structure was calculated by using the following equations :

$$1/d^2 = h^2/a^2+k^2/b^2+l^2/c^2 \qquad (4)$$

Where d is interplanar spacing a,b,c are lattice parameters and h,k,l are miller indexes

The induced strain, ε in the nanoparticle is calculated using Stokes-Wilson equation,

$$\varepsilon = \beta /4\tan\theta \text{----------} (5)$$

It is observed that the strain values show an increasing trend when pure lead oxide were doped with Co confirming the deterioration of the crystalline quality of α-PbO nano particles. The induced strain causes reduction in crystallite size and increase in peak broadening. The incorporation of small sized Co^{2+} ions in α-PbO lattice increases the strain by increasing the total grain boundary scattering. These therma stability dependent variations in crystallite size, induced strain in the lattice affect the optical properties

of α-PbO nanoparticles both the morphological and optical properties of nano particles depend upon strongly on the amount of defects. To know more on the amount of defects in the nano particle, the dislocation density, δ is calculated by using relation:

$$\delta = 1/ D^2 \text{ ---------- (6)}$$

The dislocation density Co: α-PbO increase, the increase of the dislocation density shows the degradation in the crystalline quality and the disorder of α-PbO thin film. This indicates that Co^{2+} doping deteriorate the pure α-PbO crystal structure.

Table 1 XRD analysis of pure lead oxide and doped lead oxide

sample	Position in 2θ(degre)	Position in θ(degre)	FWHM βx10^{-3} (rad)	Average d-spacing (Å)	Crystalline size D(nm)	average Crystalline size D(nm)	Avrage FWHM βx10^{-3} (rad)	Average position in (rad)	Dislocation density σx10^{-4}line/m^2	Strain in Line ^-2 m^-4	Lattice parameter (Å) a	b	c	Volume of unit cellV=a*b*c(Å^3)
α-PbO	28.6284 31.8307 48.6027	14.3142 15.9153 23.3015	4.27 2.9 3.2	2.52	32.547 47.977 43.465	41.329	3.456	0.310	5.85	0.16	2.94	2.94	5.88	50.82
Co:α-PbO	28.4357 31.8795 32.6681	14.217 15.9397 16.3340	16.5 11 9.9	2.89	8.403 12.720 15.406	12.176	12.466	0.270	6.745	0.69	2.806	2.806	5.61	44.17
Sn: α-PbO	28.6333 35.7635 48.6171	14.6316 17.8815 24.3085	4.68 4.09 3.99	2.37	29.690 33.900 34.877	32.822	4.253	0.330	9.25	0.18	2.509	2.509	5.01	31.54

Sn: α-PbO shift to the higher angle the same result were reported when Zn were doped with pbo, The shifting properties towards higher angle indicates that Zn^{+2} atoms gets substituted into the Pb^{+2} lattice sites because the major peak of zinc is around 2θ = 36. The average grain size measured from image J and average crystalline measured from the XRD of pure α-pbo is 5.50 nm and 41.329nm respectively.

This means there is a difference between grain size and crystalline size and the crystalline size were greater than grain size.

4.1.2 The UV-vis spectroscopy

The UV-vis spectroscopy measurements were taken to assess the influence of 2% Sn and Co on the pure α-PbO.

The following figure shows the reflectance spectra, the absorbance spectera and optical band gap of pure α-PbO, Sn and Co doped α-PbO sample.

The optical absorbance of the sample were determined at room temperature using Uv-visible spectrometer with in the wave length range 300 nm-800 nm. Figure 5, 6 and 7 shows the absorbation spectra for α-PbO, Sn: α-PbO and Co: α-PbO Nano particle with 2% mol of Sn and Co. The maximum absorbation spectra of pure α-pbo were at 436nm which is related to blue region. The incorporation of Sn and Co affects the absorption spectra of unadulterated α-PbO. The maximum absorbation spectra Sn: α-PbO were 387 nm which is related to violet region.The maximum absorbation spectra of Co: α-PbO were at 740 nm which is related to red region or interstial atomic defect.

The absorbation spectra of Co: α-PbO was less and the absorbation edge maximum shifts to the larger wave length from 436 to 740 nm. This shift is the indication of the decrease of the optical band gap of α-pbo nanoparticle after doping Co with 2 mol% concentration. The absorbation spectra of Sn: α-pbo and Co: α-PbO has different intensity to that the pure α-PbO and the absorbation spectra Co: α-PbO was shifted to the red shift or edge maximum were shifted to the higher wave length. This shift was the indication of the decrease in optical bandgap. The same results were reported for Mn: PbO. The absorbation spectra of Sn: α-PbO shifts to wards the blue shift. This blue shift is indicative of the decrease of crystallite size and increase in band gap. The increase in the optical band gap may be due to the decrease in crystallite size, similar results have been reported earlier [93].

The lower absorption intensity was observed for Sn and Co doped nanoparticles as compared to that of pure α-PbO nanoparticles. For 2% of Sn and Co doped α-PbO have lower density of defect levels in α-PbO matrix as compared to pure α-PbO.

The optical band gap energy of pure α-PbO and Sn and Co doped nanoparticles was analyzed using the Kubelka-Munk function relation equation [94].

$$F(R) = (1-R)^2/2R \text{ ----------(7)}$$

Where F(R) is known as kubelka–munk function and R is the reflection of the materials.

Energy band gap is the difference between the conduction bandedge minimum and the valence band edge maximum of a material. This energy band for the product sample can also be determined by drawing

graph of (F(R)*$h\nu$)^2 versus the photon energy (hν) plot. The tangent line on the curve of (F(R)*$h\nu$)^2 with the photon energy (hν) axis . The figures 8, 9 and 10 indicates that pure α-PbO, Sn and Co doped nanoparticles has the optical band gap of about 1.86 eV. From the earlier reports [95, 96, 97] the band gap depends on the preparation method and the reported band gap values were in the range 2.31-2.8 eV. We have compared the result with earlier result prepared with by spry pyrolysis techniques and the calculated band gap were 1.86eV and the earlier were 2.26eV. The calculated band gap less than earlier means the less crystalline quality due to less carrier concentration might *be* the reason for less value of band gap. The band gap of pure α-PbO were 1.86eV which is decreased to 1.46 eV for 2% Co:α-PbO. The decrease in optical band gap observed in Co doping could be related to the structural deformation in α-PbO nano particle caused due to the incorporation of Co either substitutuional or interestial Pb ion in the α-PbO lattice by Co ions in the pure α-PbO. From the XRD analysis it has been observed the crystalline size with Co doping decreases .The optical band gap of Sn: α-PbO increases as compared to pure α-PbO and the value of Sn: α-PbO were 2.6 eV for 2% Sn .The energy gap values are increased for Sn: α-PbO which may be due to the additional energy level of the dopant atom. The high band gaps valued exhibited by α-PbO as Sn doped α-PbO nanoparticle shows that this nanoparticle can be used for anti-reflection coatings of solar thermal devices and are required for any optoelectronic apllications particularly for solar cell application. For the same percentage dopant Sn and Co the band gap is varied, this means that for Co doped pure α-PbO the band gap decrease when compared to pure α-PbO and Sn: α-PbO. The bandgap energy of Co: α-PbO were smaller compared to that of pure: α-PbO and Sn: α-PbO nanoparticle.There are several factors for the decrease in optical energy band gap such as grain size, carrier concentration, structural parrameters and lattice strain and existence of defects or impurities [98,99]. There fore, the reduction in the optical band gap energy of Cobalt doped pure α-PbO is due to the induced defect energy levels near to the conduction and valence band by Co and pb ions substitu tions in lattice site of tetragonal structure.

Figure 11, 12, and 13 shows the reflectance % of the following prepared samples, such as pure α-PbO, Sn: α-PbO and Co: α-PbO. Figure 11, 12 and 13 shows as pure α-PbO and Sn: α-PbO samples have minimum reflectance in the UV region or around 400nm.where as Co: α-PbO has minimum reflectance in the red region. The percentage reflectance of the pure lead oxide is greater than the doped one, the percentage reflectance of pure α-PbO greater than both Co and Sn. The percentage reflectance of pure α-PbO around 84% where as the percentage reflectance of tin and cobalt doped with pure α-PbO were around 58% and 62% respectively. Pure α-PbO were exibit the maximum reflectance at 740 nm which is related to the red region and minimum reflectance at 436nm which is related to blue region.The

maximum reflectance of pure α-PbO doped with 2 % of Sn and Co doing were observed at around 600-700 nm and 605-615nm respectively and the minimum reflectance of Sn and Co doped with pure α-PbO were 613nm which is related to orange region or interestial atomic defect and at 529 nm and 740 nm which is related to green region or single ionized region and red region respectively. The graph of reflectance vs wave length from the figure 5 shows the reflectance spectra of pure lead oxide nano particle with in the wave length range 300 nm- 800 nm. Pure α-PbO can be seen that high reflectance percentage compared to that of Sn: α-PbO and Co: α-PbO. The reflectance spectra of Sn: α-PbO and Co: α-PbO nano particle with in molar ratio of 2% Sn & Co with in the wave length 300 nm-800 nm. Doped nanoparticle can be seen that decrease in optical reflectance when compared to the undoped.

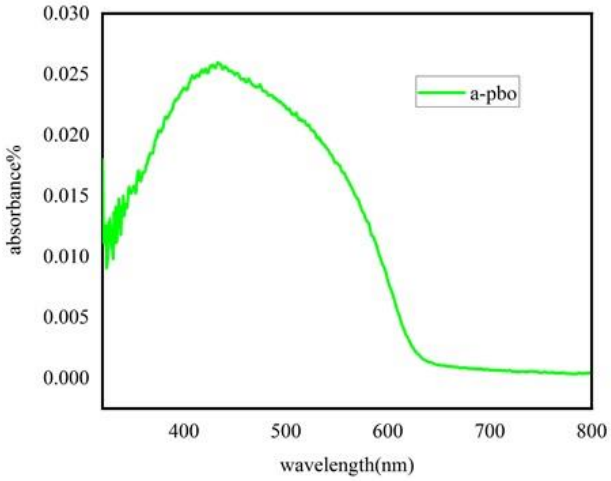

Figure 5 the absorbance spectra of pure of α-PbO**,**

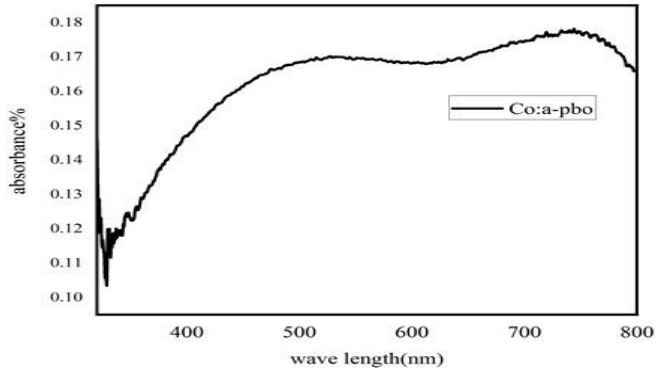

Figure 6 the absorbance spectra of Co:α-PbO

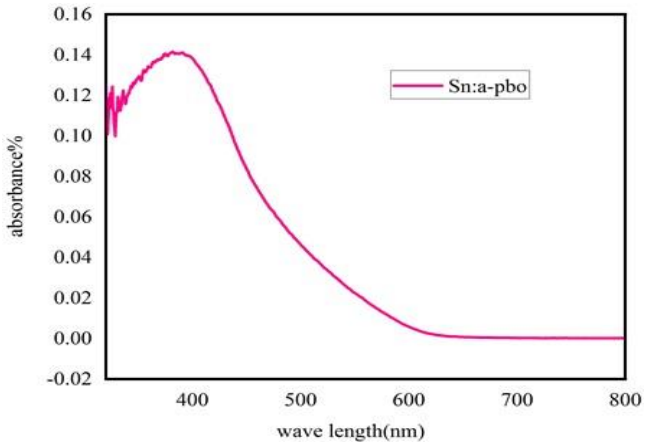

Figure 7 the absorbance spectra of Sn:α-PbO

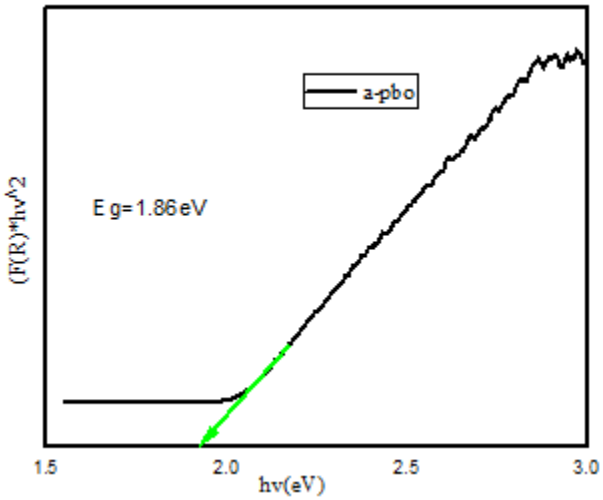

Figure 8 the energy bandd gap of pure α-PbO

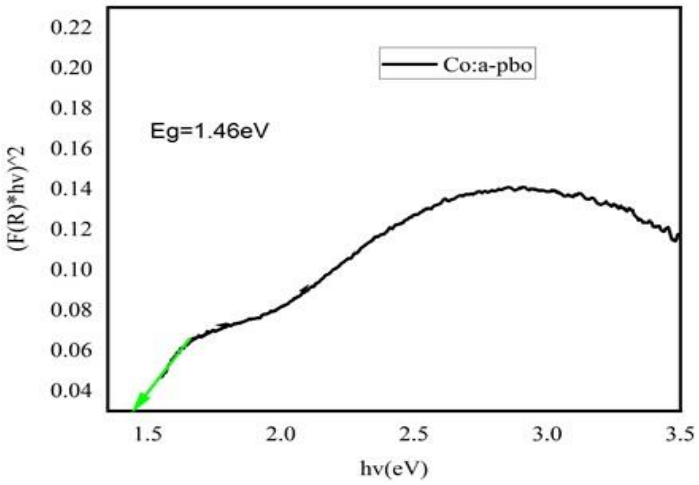

Figure 9 the energy band gap of Co: α-PbO

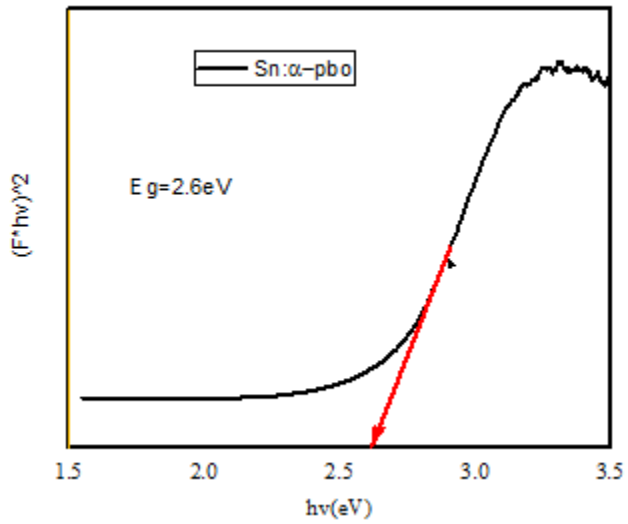

Figure 10 energy band gap of Sn: α-PbO

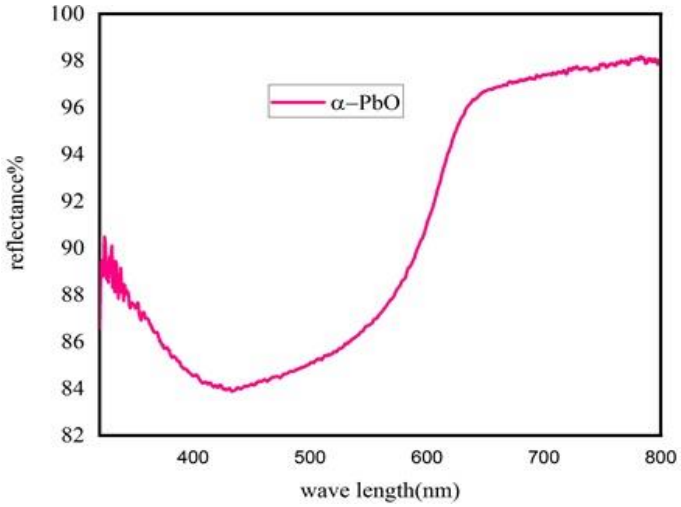

Figure 11 reflectance spectra of pure α-PbO

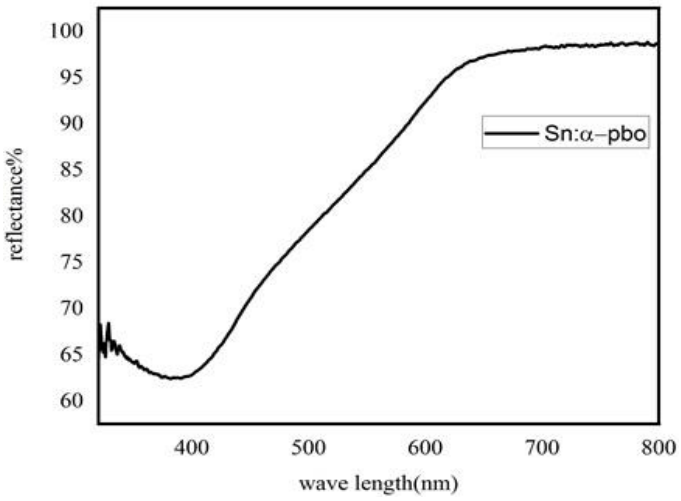

Figure 12 the reflectance spectra of tin doped pure α-PbO

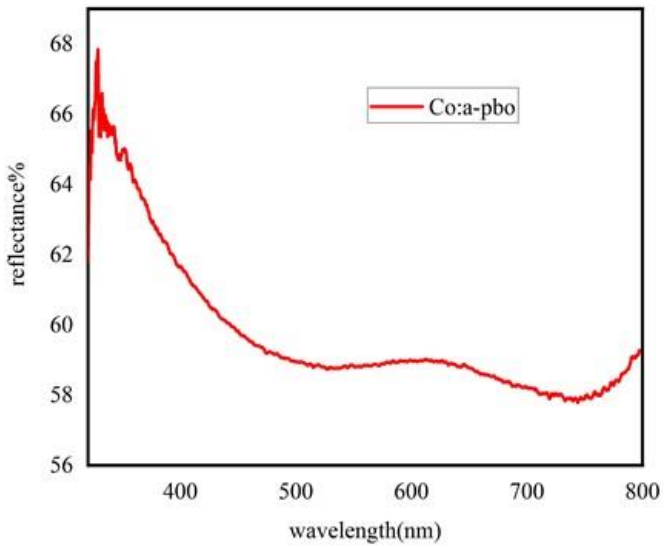

Figure 13 the reflectance spectra of cobalt doped pure α-PbO

4.1.3 Photoluminescence

As shown in Figure 14 and 15 the room-temperature photo luminescence emission spectra of the prepared samples at an excitation wavelength of 350 & 415 nm. The emission spectra of pure α-PbO, 2% Co and Sn doped with α-PbO at excitation wave length of 350nm and 415nm shows different properties because the incorporation of Sn and Co affects the emmision spectra of prepared sample α-PbO, 2% Sn: α-PbO nanoparticles.The emission spectra of α-PbO, 2% Co and Sn doped with α-PbO at excitation wave length of 350nm are all in the viole region and the emission spectra of α-PbO, 2% Co and Sn doped with α-PbO at excitation wave length of 415nm are all in the green region.

Localized defects from the nanoparticle can act as traps for excitons or charge carriers .These defect caninfluence the photoluminesce intensity by either quenching or enhancing emission on their nature and location. The photoluminescence intensity observed at 439 nm can be assigned recombination of free excitons which are referred to as near band edge emission (NBE) [100]. The emission spectra of pure α-pbo 2% Sn: α-PbO and 2% Co: α-PbO, nanoparticles were exhibited strong emission peaks centered at 439 nm related to violet emission at excitation wave length 350 nm. Emission at wave length 437nm and 434 nm are at violet emission. A broad photoluminescence emission has already observed from the localized surface state of pure α-PbO in the range of 350-475 nm, the broad peak centered at 437nm and 439nm appeared in Co: doped pure α-PbO Nano particles. This emission peaks may be due to an electron

transition in α-PbO band gap mediated by the defect energy level generated from oxygen vacancies and lead. Emission spectra of pure α-PbO 2% Sn: α-PbO and Co: α-PbO nanoparticles at excitation wave 415 nm length all lies at emission. The green emission peak at 505 & 506 nm due to the recombination of electron with hole traped in the single ionized lead vacancies [101]. Pure α-PbO emission at 505 nm 2% Co: α-PbO emission at 505 nm and 2% Sn: α-PbO emission at 506 nm. The maximum luminescence intensity of the synthesized sample transitions from 439 nm to 505 nm, indicating a shift from violet to green region. Pure α-PbO and Sn: α-PbO exhibits a lower luminescence intensity than Co: α-PbO. Lower luminescence intensity means a smaller fraction of absorbed photon energy were re-emited. High emission intensity means high re-combination rate. From the Figure 14 and 15 below at a wave length of 350 nm & 415 nm Co: α-PbO has higher luminescence intensity than pure α-PbO and Sn: α-PbO this means Co: α-PbO has high emission intensity and high emission intensity means high re-combination rate or greater proportion of absorbed photon energy are re-emited.

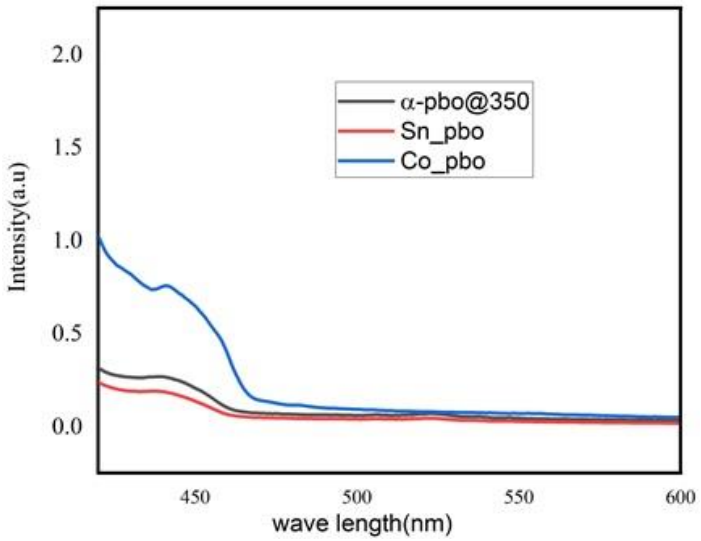

Figure 14 photoluminescence spectra of pure α-PbO, Sn: α-PbO and Co: α-PbO at excitation wave length of 350 nm

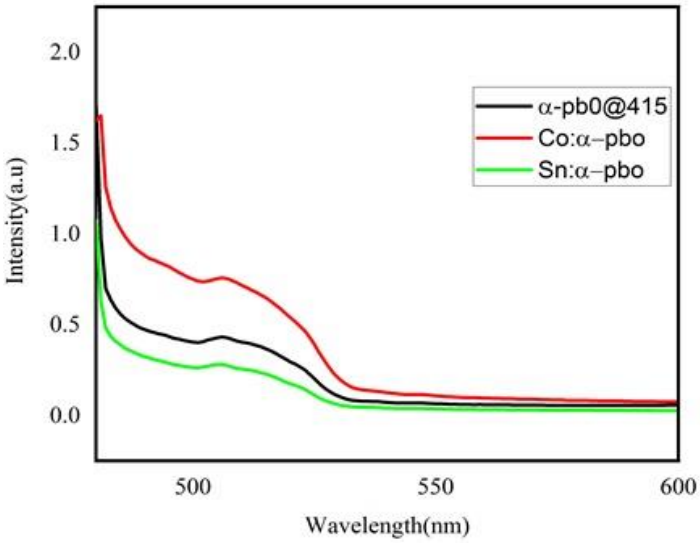

Figure 15 photoluminescence spectra of pure α-PbO, Sn: α-PbO and Co: α-PbO at excitation wave length of 415 nm

4.1.4 Energy dispersive x-ray (EDXs) analysis

The energy dispersive x-ray spectrum confirms the presence of Pb and O element in the α-PbO sample which demonstrates the high purity of nano particle synthesized by co-precipitation method.The atomic percentage of Pb: O is 45.26 O to 54.74 Pb atoms. They have nearly the same atomic ratio. The elemental compositions of Pb, Co, Sn and O in the synthesized nanoparticle were measured from energy dispersive x-ray. The energy dispersive x-ray analysis doped Sn: α-PbO, Co: α-PbO in figure 16, 17 and 18 confirms that the presence of Sn, Co, Pb and O. The as deposited ternary nanoparticle that were Sn: α-PbO and Co: α-PbO when consider atomic percentage Sn: Pb: O and Co: Pb: O is 0.62:53.60:45.78 and 24.44:29.68:45.88 respectively. The obtained plate confirms the presence of Pbo , Sn and Co with condition voltage of 40Kv , current of 30A and 40 % of NaoH a as electrolyte . The cobalt and tin present were 2% by weight. For the same 2 % tin and cobalt by weight the atomic percentage of doped atom becomes different .When considered the atomic % of pb, Sn, Co and O present in the spectra the atomic % of O in both pure α-PbOand Sn: α-PbO , Co: α-PbO were nearly the same but the atomic % of Sn and Co becomes different. As observed from the table 3 and 4 for the same 2mol% of Sn and Co the atomic % of Co were 24.44 and Sn were 0.63.There for the atomic % of Sn were less than the atomic % of Co. As shawn in EDX spectrum Sn:α-PbO and Co:α-PbO for 2 % of Sn & Co in α-PbO along with un doped α-PbO is shown in Figure 16,17 and18 the EDX spectrum reveals the presence of Sn,Co,Pb and O in the α-PbO,Sn:α-PbO and Co:α-PbO nanoparticle.

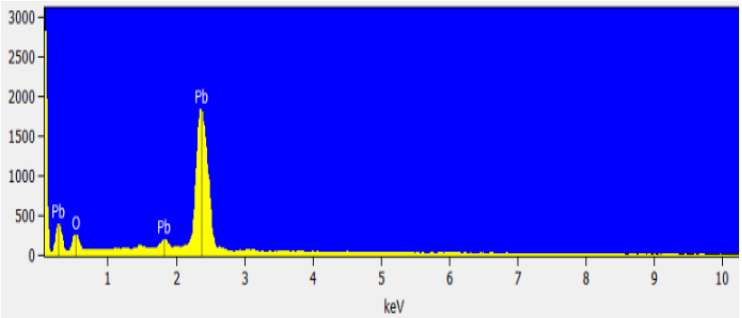

Figure 16 EDX image of pure lead oxide

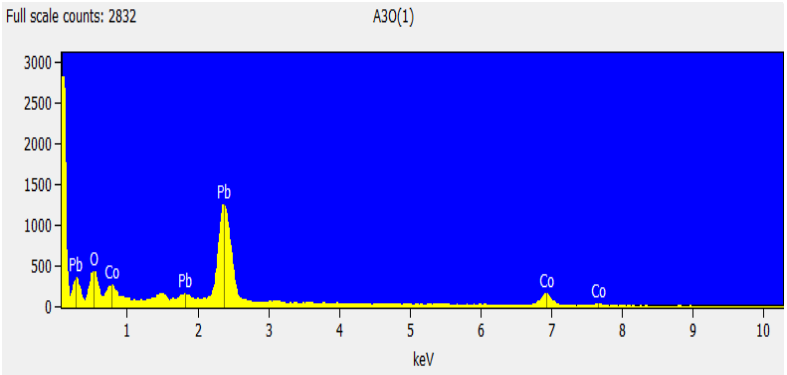

Figure 17 EDX image of Cobalt doped pure lead oxide

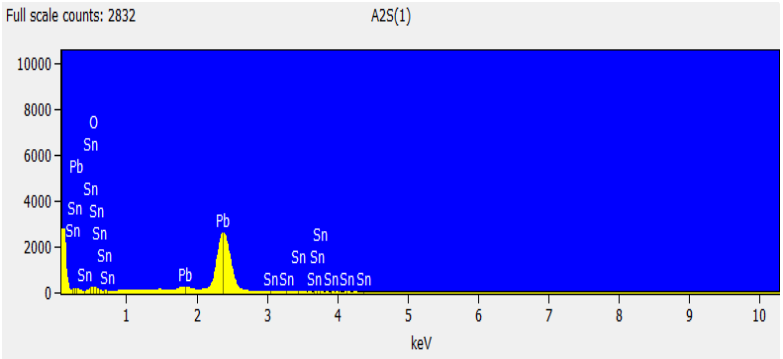

Figure 18 EDX image of tin doped pure lead oxide

Table 2 Elemental composition of pure lead oxide nanoparticles

Element line	Weight %	Atomic %
O k	**6**	**45.26**
Pb L	**--**	
Pb M	**94**	**54.74**
Total	**100**	**100**

Table 3 Elemental composition of tin doped pure lead oxide nano particles

Element line	Weight %	Weight error %	Atom %	Atom error %
O k	**6.15**	**0.56**	**45.78**	**4.16**
Sn K	**0.62**	**0.39**	**0.62**	**0.39**
Sn M	**-**	**-**	**-**	**-**
Pb L	**-**	**-**	**-**	**-**
Pb M	**93.23**	**1.12**	**53.60**	**0.65**
Total	**100.00**		**100.00**	

Table 4 Elemental composition of cobalt doped pure lead oxide nano particles

Element line	Weight %	Weight error %	Atom %	Atom error %
O K	**8.82**	**0.90**	**45.88**	**4.71**
Co K	**17.30**	**0.67**	**24.44**	**0.94**
Co L	**-**	**-**	**-**	**-**
Pb L	**-**	**-**	**-**	**-**
Pb M	**73.88**	**1.21**	**29.68**	**0.49**
Total	**100**		**100**	

4.1.5 Scanning electron microscopy (SEM) ananlysis

The SEM images of un-doped and Sn and Co doped α-PbO nanoparticles are shown in Figure 19, 20 and 21. Un doped α-PbO and Sn:α-PbO samples exhibit similar morphology but, Co doped α-PbO exhibit's different morphology, the amount of agglomeration or index of crystallinity differs.The morphology result of pure α-PbO, 2% Sn: α-PbO and 2% Co: α-PbO nanoparticle are shown in the figure 19, 20, and 21 respectively. As demonstrated in the figure below the morphology of α-PbO and Sn: α-PbO is non uniform and high loosely packed and the particles were less clearly agglomerated in SEM image. From the SEM image it is easily observed that doping with Co play significant role on the morphological nature of the nanocrystalline of the prepared sample. Pure α-PbO and Sn doped α-PbO shows irrgular shaped morphology with slight agglomeration and are bigger and more loosely packed and no effect on morphology of nanoparticles. But when Cobalt is added to a pure α-PbO there is a morphology change and have homogeneous microstructure with less loosely packed, irregular shape and small size as compare pure α-PbO and Sn doped α-PbO. Hence, it can be concluded that the addition of Co in α-PbO system enhances the particle morphology change with less defined crystallinity. The average particle size distribution of α-PbO, 2%Co, doped α-PbO was obtained by analyzing the SEM image using the software ImageJ as shown in figures 21. The histograms represent α-PbO nanoparticles with an average diameter of about 32 nm. However, the addition of Co^{2+} influence the size morphology in which of average particles size distribution of the nanoplates is decreased from 32 nm to 37 nm due to divalent cobalt ions restrict the growth of α-PbO and lead to growing in the nanoplate direction [102] . This decreased the average diameter which is a good agreement with average crystalline size calculated from the XRD.

.

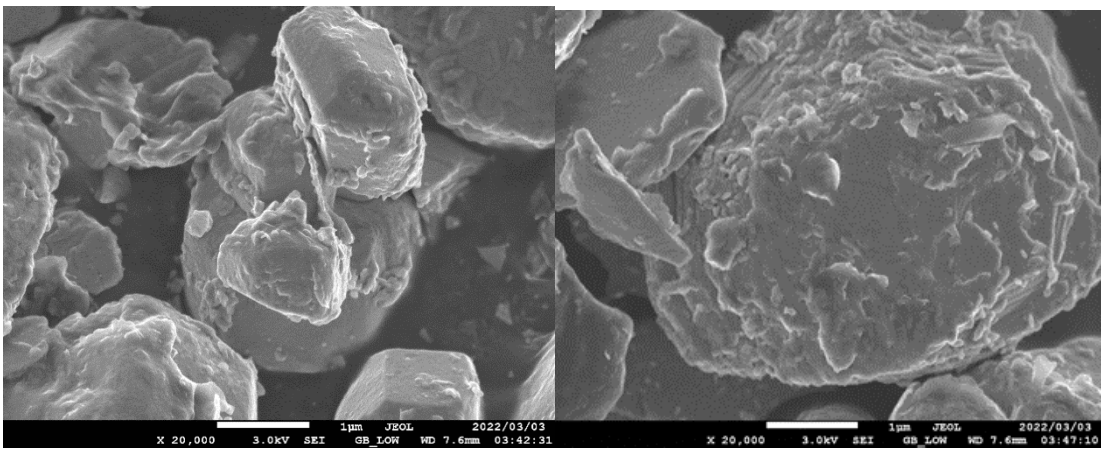

Figure 19 SEM image of pure α-PbO nanoparticles at diferent magnification

2

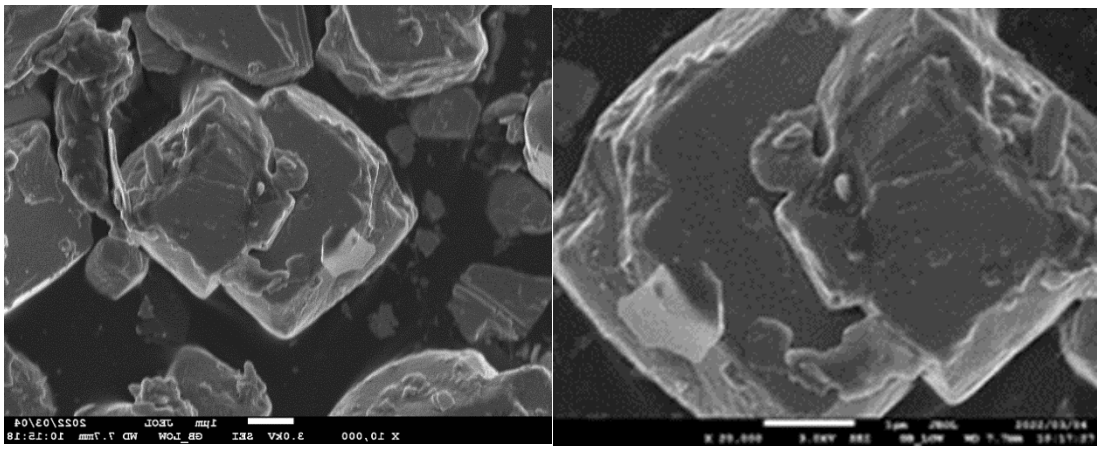

Figure 20 SEM image of tin doped pure α-PbO nanoparticles at diferent magnification

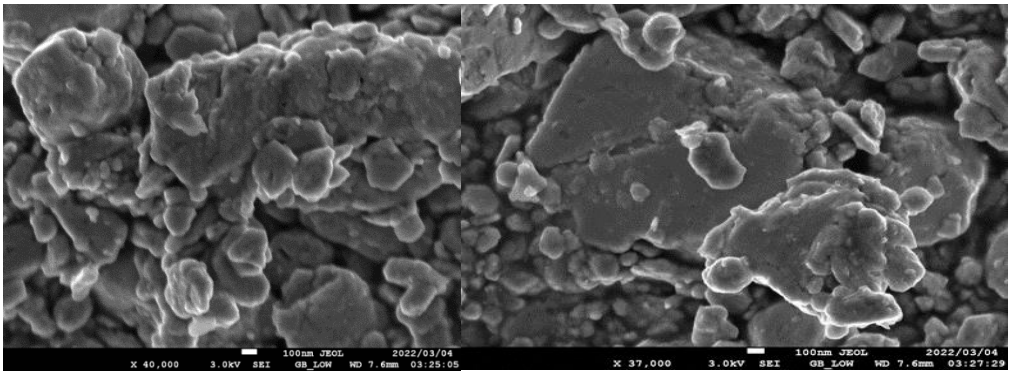

Figure 21 SEM image of cobalt doped pure α-PbO nanoparticles at diferent magnification

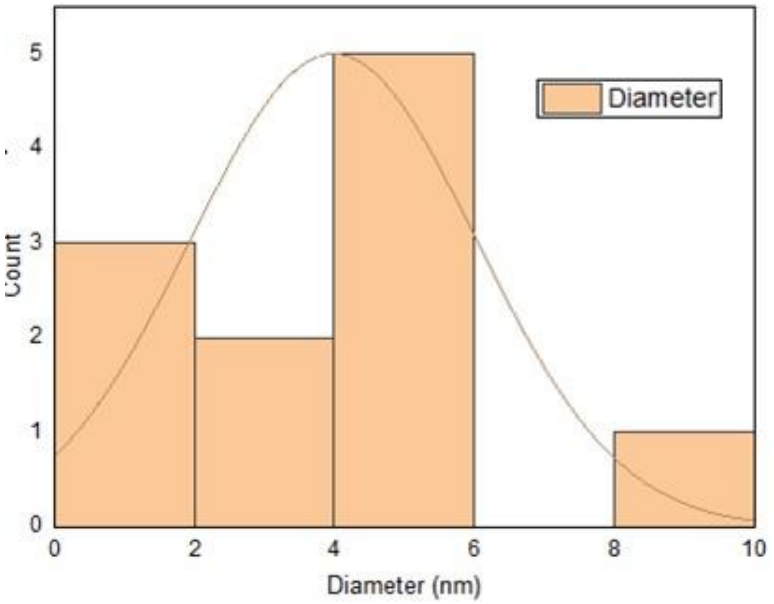

Figure 22 the average grain size of α-PbO nanoparticles

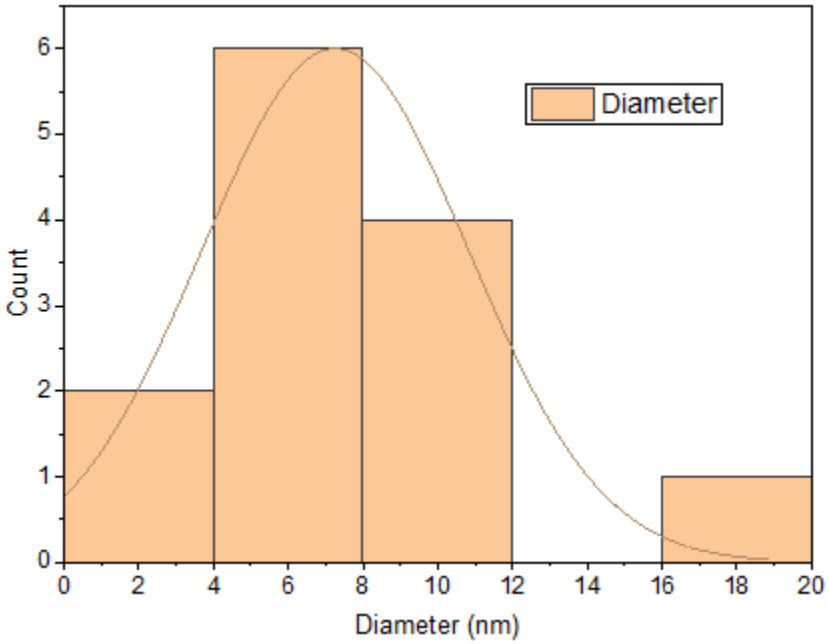

Figure 23 the average grain size of tin doped pure α-PbO nanoparticles

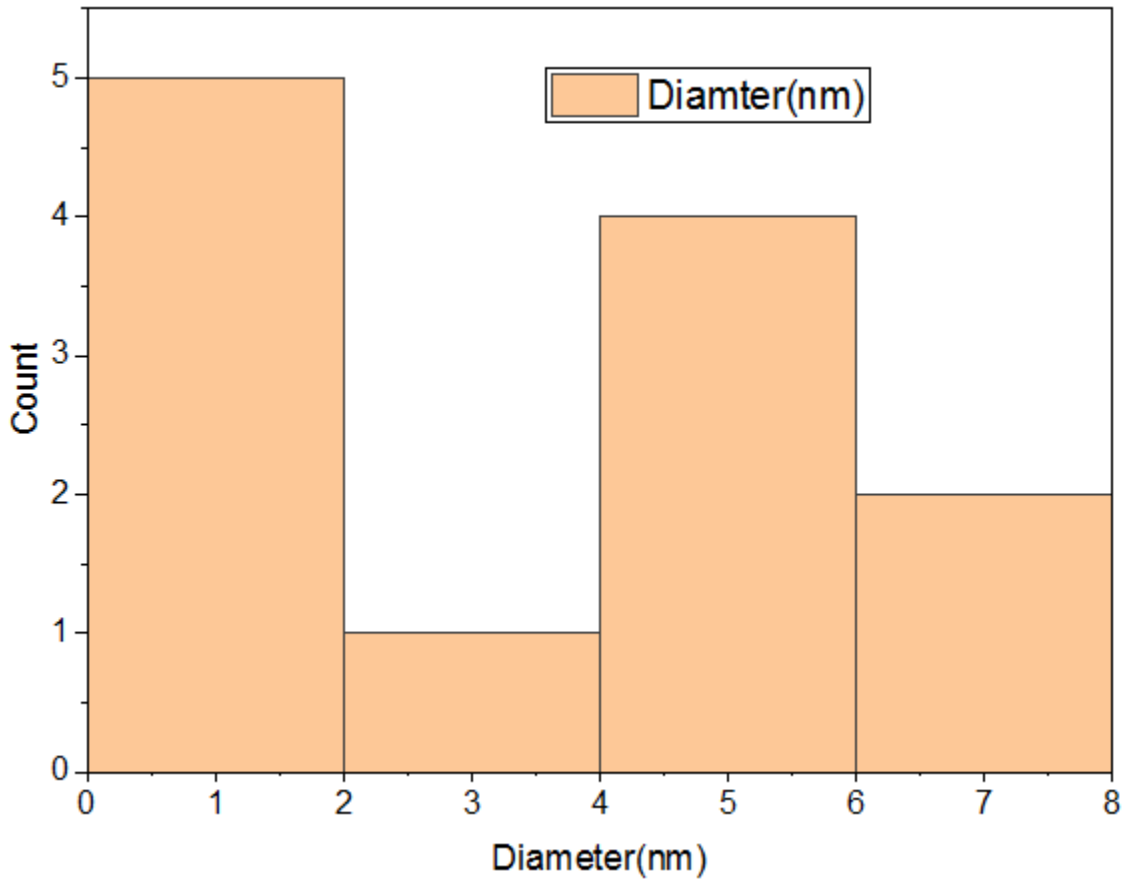

Figure 24 the average grain size of cobalt doped pure α-PbO nanoparticles

5. Conclusion

The present work has focused on synthesizing and characterizing the structural and optical properties of pure α-PbO, Sn:α-PbO, and Co:α-PbO. In a recent study, pure and doped α-PbO nanoparticles were synthesized via chemical precipitation. XRD analysis showed that the crystallinity and peak positions of Sn:α-PbO improved compared to pure α-PbO, while those of Co:α-PbO decreased. The crystallite sizes were 43.47 nm for pure α-PbO, 13 nm for Sn:α-PbO, and 35.12 nm for Co:α-PbO. Sn and Co doping reduced the crystallite size. XRD also revealed shifts in the (111) peak: Co:α-PbO shifted to lower angles, while Sn:α-PbO shifted to higher angles. UV-vis spectroscopy indicated that the optical band gap of pure α-PbO was 1.86 eV, decreasing to 1.46 eV for 2% Co:α-PbO and increasing to 2.6 eV for 2% Sn:α-PbO. The blue shift in Sn:α-PbO and the red shift in Co:α-PbO's absorption spectra suggest changes in band gap and crystallite size. EDX analysis confirmed the presence of Sn, Co, Pb, and O without extraneous elements, with atomic percentages of 00.62:53.60:45.78 for Sn:α-PbO and 24.44:29.68:45.88 for Co:α-

PbO. PL emission spectra showed strong violet peaks at 439 nm for all samples. SEM images revealed cubic morphology in pure and Sn-doped α-PbO, while Co-doping altered the morphology. The average grain size from SEM was 5.50 nm, whereas XRD gave a crystallite size of 41.33 nm, indicating a discrepancy between grain and crystallite sizes.

6. Recomendation

Future studies should conduct to investigate Sn, Co doped with pure PbO for better under standing of Electrical properties of the nanoparticles.

References

[1]. Babu, S. Harinath, S. Kaleemulla, N. Madhusudhana Rao, and C. Krishnamoorthi. "Indium oxide: A transparent, conducting ferromagnetic semiconductor for spintronic applications." *Journal of Magnetism and Magnetic Materials* 416 (2016): 66-74.

[2]. Krataitong, Chutimun, Kitima Srichai, and Auttasit Tubtimtae. "Structural and optical properties of undoped and antimony-doped lead telluride thin films." *Materials Letters* 285 (2021): 129085.

[3] .Boon-on, Patsorn, Cing-Ru Chiang, Raja Rajendran, Nipapon Suriyawong, Jen-Bin Shi, and Ming-Way Lee. "Pb5Sb8Se17-δ nanocrystals: A new solar absorber material with an optimal bandgap and an efficiency near 6% under 0.05 sun." *Journal of Power Sources* 485 (2021): 229324.

[4]. Tubtimtae, Auttasit, Prayoonsak Pluengphon, and Burapat Inceesungvorn. "Indium dopant-induced morphological and optical properties of tin-antimony sulfide thin films synthesized by the spin coating method compared with ab initio calculation." *Materials Letters* 300 (2021): 130140.

[5]. Oliveira, Aline A., Marlon I. Valerio-Cuadros, Lilian FS Tupan, Vitor Santaella Zanuto, Flávio F. Ivashita, and Andrea Paesano Jr. "Fe-doped In2O3 nanostructures synthesized via a freeze-drying process: structural and optical properties." *Materials Letters* 250 (2019): 210-213..

[6] Oliveira, Aline A., Marlon I. Valerio-Cuadros, Lilian FS Tupan, Vitor Santaella Zanuto, Flávio F. Ivashita, and Andrea Paesano Jr. "Fe-doped In2O3 nanostructures synthesized via a freeze-drying process: structural and optical properties." *Materials Letters* 250 (2019): 210-213.

[7] Droessler, Laura M., Hazel E. Assender, and Andrew AR Watt. "Thermally deposited lead oxides for thin film photovoltaics." *Materials Letters* 71 (2012): 51-53.

[8] . Thangaraju, B., and P. Kaliannan. "Optical and structural studies on spray deposited α-PbO thin films." *Semiconductor science and technology* 15, no. 6 (2000): 542.

[9] Chen, Kuang-Cai, Chang-Wei Wang, Yong-Ill Lee, and Hong-Guo Liu. "Nanoplates and nanostars of β-PbO formed at the air/water interface." *Colloids and surfaces A: physicochemical and engineering aspects* 373, no. 1-3 (2011): 124-129.

[10]. Chandrika, B. M., H. C. Manjunatha, L. Seenappa, R. Munirathnam, K. N. Sridhar, S. Manjunatha, and AJ Clement Lourduraj. "Aloe vera-mediated green synthesis of bismuth-zinc-iron nanocomposite for radiation shielding applications." *Journal of Physics and Chemistry of Solids* 181 (2023): 111538.

[11] S. K. Pasha, K. Chidambaram, N. Vijayan, W. Madhuri, Structural and electrical properties of nano structure lead oxide, Optoelect. Adv. Mater. Rapid Comm. 6 (2012) 110.nedy, J. J. Vijaya, Lead oxide - PbO humidity sensor, Sensors and Trasducers Journal 122 (11) (2010) 113

[12]0 M. Martos, J. Morales, L. Sanchez, R. Ayouchi, D. Leinen, F. Martin, J. R. Barrado, Electrochemical properties of lead oxide films obtained by spray pyrolysis as negative electrodes for lithium secondary batteries, Electrochimica Acta 46 (2001) 2939.

[13] Q. Li, C. Feng, Electrochemical performance of nanostructured PbO@C obtained by solgel method, J. Electron. Mater. 45 (6) (2016) 3127.

[14] A. Tubtimtae, P. Pluengphon, B. Inceesungvorn, Mater. Lett. 300, 130140 (2021).

[15] D. Raknual, S. Charoenphon, P. Reunchan, A. Tubtimtae, Electrochim. Acta 389, 138773 (2021).

[16] A. A. Oliveira, M. I. Valerio-Cuadros, L. F. S. Tupan, V. S. Zanuto, F. F. Ivashita, A. Paesano Jr., Mater. Lett. 250, 210 (2019).

[17]. Droessler, Laura M., Hazel E. Assender, and Andrew AR Watt. "Thermally deposited lead oxides for thin film photovoltaics." *Materials Letters* 71 (2012): 51-53.

[18]. Thangaraju, B., and P. Kaliannan. "Optical and structural studies on spray deposited α-PbO thin films." *Semiconductor science and technology* 15, no. 6 (2000): 542.

[19]. Chen, Kuang-Cai, Chang-Wei Wang, Yong-Ill Lee, and Hong-Guo Liu. "Nanoplates and nanostars of β-PbO formed at the air/water interface." *Colloids and surfaces A: physicochemical and engineering aspects* 373, no. 1-3 (2011): 124-129.

[20]. Suryawanshi, V. N., Ashwini S. Varpe, and Mrinalini D. Deshpande. "Band gap engineering in PbO nanostructured thin films by Mn doping." *Thin Solid Films* 645 (2018): 87-92.

[21]. A. B. Velichenko, R. Amadelli, E. A. Baranova, D. V. Girenko, F.I. Danilov, J. Electroanal. Chem. 527, 56 (2002). [22] W. Zhang, Y. Xie, J. Gu, S. Ai, J. Wang, K. Yamamoto, L. Jin, Analyst 129, 229 (2004).

[23]. Xia, Yijing, Qizhou Dai, and Jianmeng Chen. "Electrochemical degradation of aspirin using a Ni doped PbO2 electrode." *Journal of Electroanalytical Chemistry* 744 (2015): 117-125.

[24] M. Azarang, M. Aliahmad, A. G. Shiravizadeh, H. R. Azimi, R. Yousefi, J. Appl. Phys. 124, 123101 (2018).

[25]. Kashani-Motlagh, Mohammad Mehdi, and Masoumeh Karami Mahmoudabad. "Synthesis and characterization of lead oxide nano-powders by sol–gel method." *Journal of sol-gel science and technology* 59 (2011): 106-110.

[26]. Eya, D. D. O. "Influence of thermal annealing on the structural and optical properties of PbO thin films prepared by chemical bath deposition technique." *Pacific Journal of Science and Technology* 7, no. 2 (2006): 114-119.

[27]. Zhang, Weiying, Jianguo Zhao, Zhenzhong Liu, Zhaojun Liu, and Zhuxi Fu. "Influence of growth temperature of TiO2 buffer on structure and PL properties of ZnO films." *Applied Surface Science* 256, no. 14 (2010): 4423-4425.

[28]. Jafari-Rad, Ali, and Hosein Kafashan. "Preparation and characterization of electrochemically deposited nanostructured Ti-doped ZnS thin films." *Ceramics International* 45, no. 17 (2019): 21413-21422.

[29]. Mazhdi, M., and KHANI P. HOSSEIN. "Structural characterization of ZnO and ZnO: Mn nanoparticles prepared by reverse micelle method." (2012): 233-240.

[30] .Slater, John C. "Atomic radii in crystals." *The Journal of Chemical Physics* 41, no. 10 (1964): 3199-3204.

[31]. A. Nakrela, N. Benramdane, A. Bouzidi, Z. Kebbab, M. Medles, C. Mathieu, Results Phys. 6, 133 (2016).

[32].Sathya, M., and K. Pushpanathan. "Synthesis and optical properties of Pb doped ZnO nanoparticles." *Applied Surface Science* 449 (2018): 346-357.

[33]. N. B. Hasan, M. A. Mohammed, Electrical properties of (PbO)1−x (CdO)x thin films fabricated by spray pyrolysis technique, Adv. Appl. Sci. Res. 6 (7) (2015) 116.

[34] A. O. Mousa, A. F. Marmoss, Effect of substrate temperature on structyral and optical properties of PbO thin films deposited by chemical spray pyrolysis technique, Int. J. Phara. Chem. Bio. Sci. 6 (4) (2016) 356.

[35] P.U. Asogwa, Bang gap shift and optical characterization of PVA capped PbO thin films: effect of thermal annealing, Chalcigenide Letters, 8 (3) (2011) 163.

[36] M. Suganya, N. Narasimman, H. J. Srivind, V. S. Nagarethinam, K. Usharani, A. R. Balu, Studies on the physical properties of spray and silar deposited lead oxide thin films, J. Electron Devices 21 (2015) 1842.

[37] M. Suganya, A. R. Balu, K. Usharani, Role of substrate temperature on the growth mechanism and physical properties of spray deposited lead oxide thin films, Materials Science-Poland 32 (3) (2014) 448.

[38] M. K. Mahmoudabad, M. M. Kashani-Motlagh, Synthesis and characterization of PbO nanostructure and NiO doped with PbO through combustion of citrate/nitrate gel, Int. J. Physi. Sci. 6 (24) (2011) 5720.

[39A. V. Borhade, D. R. Tope, B. K. Uphade, An Efficient Photocatalytic Degradation of Methyl blue dye by using synthesised PbO nanoparticles. E-J. Chem. 9 (2) (2012) 705.

[40] N. Mythili, K. T. Arulmozhi, A comparative study on the structural and optical properties of PbO and Zn doped PbO nanocrystals, J. Mater. Sci: Mater. Electron. 25 (2014) 3984.

[41] L. Zhou, X. Li, Z. Yao, Z. Chen, M. Hong, R. Zhu, Y. Liang, J. Zhao, Transition-metal doped ceria microspheres with nanoporous structures for CO oxidation, Scientific Reports, 6 (2016) 23900.

[42] G. H. Mhlongo, K. Shingange, Z. P. Tshabalala, B. P. Dhonge, F. A. Mahmoud, B. W. Mwakikunga, D. E. Motaung, Room temperature ferromagnetism and gas sensing in ZnO nanostructures: Influence of intrinsic defects and Mn, Co, Cu doping, Appl. Surf. Sci. 390 (2016) 804.

[43] B. Kharroubi, R. Baghdad, A. Abdiche, M. Bousmaha, M. Bousquet, A. Zeinert, M. E. Marssi, K. Zellama, S. Hamzaoui, Mn doping effect on the structural properties of ZnO-nanostructured films deposited by the ultrasonic spray pyrolysis method, Phys. Scr. 86 (2012) 015805.

[44] I. Akyuz, S. Kose, S. Atay, V. Bilgin, The optical, structural and morphological properties of ultrasonically sprayed ZnO:Mn films, Semicond. Sci. Technol. 21 (2006) 1620.

[45]. N. Manjula, M. Pugalenthi, V. S. Nagarethinam, K. Usharani, A. R. Balu, Effect of doping concentration on the structural, morphological, optical and electrical properties of Mn-doped CdO thin films, Mater. Sci. Poland 33 (4) (2015) 774.

[46]. N. Manjula, A. R. Balu, K. Usharani, N. Raja, V. S. Nagarethinam, Enhancement in some physical properties of spray deposited CdO:Mn thin films through Zn doping towards optoelectronic applications, Optik 127 (2016) 6400.

[47] K. Sankarasubramanian, P. Soundarrajan, T. Logu, S. Kiruthika, K. Sethuraman, R. R. Babu, K. Ramamurthi, Influence of Mn doping on structural, optical and electrical properties of CdO thin filmsprepared by cost effective spray pyrolysis method, Material Science in Semiconductor Processing 26 (2014) 346.

[48] A. M. Sayed, A. Ibrahim, Structural and optical characterizations of spin coated cobalt-doped cadmium oxide nanostructured thin films, Material Science in Semiconductor Processing 26 (2014) 320.

[49] .Y. Gulen, F. Bayansal, B. Sahin, H. A. Cetinkara, H. S. Guder, Fabrication and characterization of Mn-doped CuO thin films by the SILAR method, Ceramics International 39 (2016) 6475.

[50] . Noguera, C. Physics and Chemistry at Oxide Surfaces; Cambridge University Press: Cambridge, UK, 1996

[51], Kung, H.H. Transition Metal Oxides: Surface Chemistry and Catalysis; Elsevier: Amsterdam, 1989.

[52].. Wyckoff, R.W.G. Crystal Structures, 2nd ed; Wiley: New York, 1964

[53] Ayyub, P.; Palkar, V.R.; Chattopadhyay, S.; Multani, M.; Phys. Rev. B. 1995, 51, 6135.

[54] Zhang, H.; Bandfield, J.F.; J. Mater. Chem. 1998, 8, 2073.

[55]. Samsonov, V.M.; Sdobnyakov, N.Yu.; Bazulev, A.N. Surf. Sci. 2003, 532-535, 526.

[56] Song, Z.; Cai, T.; Chang, Z.; Liu, G.; Rodriguez, J.A.; Hrbek, J. J. Am. Chem. Soc. 2003, 125, 8060.

[57]. Rodriguez, J.A.; Rodriguez, L.; Ruette, F.; Gonzalez, L. in preparation.

[58]. Ayyub, P.; Multani, M.; Barma, M.; Palkar, V.R.; Vijayaraghavan, R. J. Phys. C: Solid State Phys. 1988, 21, 229. [59]. Garvie, R.C.; Goss, M.F. J. Mater. Sci. 1986, 21, 1253.

[60]. Hernández-Alonso, M.D.; Hungría, A.B.; Coronado, J.M.; Martínez-Arias, A.; Conesa, J.C.; Soria, J.; Fernández-García, M.; Phys. Chem. Chem. Phys. 2004, 6, 3524.

[61]. Skandan, G., C. M. Foster, H. Frase, M. N. Ali, J. C. Parker, and H. Hahn. "Phase characterization and stabilization due to grain size effects of nanostructured Y2O3." *Nanostructured Materials* 1, no. 4 (1992): 313-322.

[62]. ernández-García, Marcos, Jose Carlos Conesa, and Francesc Illas. "Effect of the Madelung potential value and symmetry on the adsorption properties of adsorbate/oxide systems." *Surface science* 349, no. 2 (1996): 207-215

[63].Rodriguez, J.A.; Chaturvedi, S.; Kuhn, M.; Hrbek, J. J. Phys. Chem. B, 1998, 102, 5511.

[64] Hoffmann, R. Solids and Surfaces: A Chemist's View of Bonding in Extended Structures; VCH: New York, 1988.

[65].Albright, T.A.; Burdett, J.K.; Whangbo, M.H. Orbital Interactions in Chemistry; Wiley-Interscience: New York, 1985

[66]. Rodríguez, J.A., Fernández-García, M; (Eds.) Synthesis, Properties and Applications of Oxide Nanoparticles. Whiley: New Jersey, 2007.

[67]. Mather, G.C.; Martinez-Arias; A.; Transport properties and Oxygen Handling in "Synthesis, Properties and Applications of Oxide Nanoparticles" (Rodríguez, J.A., Fernández-García, M; Eds.). Whiley: N.J., 2007. Chpt. 13.

[68].Föller, A.M. Magnesium Oxide and its Applications; Vollhardt: Berlin, 1978.

[69]. Tasker, P. W. "Structure and properties of MgO and Al2O3 ceramics." *Advances in ceramics* 10 (1984): 176.

[70]. Gibson, A.; Haydock, R.; LaFemina, J.P. J. Vac. Sci. Technol. A 1992, 10, 2361.

[71].Stener, M.; Fronzoni, G.; De Francesco, R. Chem. Phys. 2005, 309, 49.

[72]. Moodie, A. F., and C. E. Warble. "Electron microscopic investigations of MgO morphology and surfaces." *Journal of Crystal Growth* 10, no. 1 (1971): 26-38.

[73]. Mackrodt, W. C. "Classical and quantum simulation of the surface properties of α-Al2O 3." *Philosophical Transactions of the Royal Society of London. Series A: Physical and Engineering Sciences* 341, no. 1661 (1992): 301-312.

[74]. Ambrosino, Fabio, A. Antonelli, M. Antonelli, C. Bacci, P. Beltrame, G. Bencivenni, S. Bertolucci et al. "Study of the decay $\phi \rightarrow f0(980)\gamma \rightarrow \pi^+\pi^-\gamma$ with the KLOE detector." *Physics Letters B* 634, no. 2-3 (2006): 148-154..

[75]. Trovarelli, A. Catal. Rev. Sci.- Eng. 1996, 38, 439.

[76]. Rodriguez, J.A.; Hanson, J.C.; Kim, J.-Y.; Liu, G.; Iglesias-Juez, A.; FernándezGarcía, M. J. Phys. Chem. B, 2003, 107, 3535.

[77]. Fu, Q.; Saltsburg, H.; Flytzani-Stephanopoulos, M. Science, 2003, 301, 935.

[78]. Fernández-García, M.; Martínez-Arias, A.; Guerrero-Ruiz, A.; Conesa, J.C.; Soria, J. J. Catal. 2002, 211, 326.

[79]. Vlaic, G.; Di Monte, R.; Fornasiero, P.; Fonda, E.; Kašpar, J.; Graziani, M. J. Catal. 1999, 182, 378.

[80]. Liu, W.; Wadia, C.; Flytzani-Stephanopoulos, M. Catal. Today, 1996, 28, 391.

[81]. Rodriguez, J.A.; Jirsak, T.; Freitag, A.; Hanson, J.C.; Larese, J.Z.; Chaturvedi, S. Catal. Lett. 1999, 62, 113.

[82]. Fu, Q.; Weber, A.; Flytzani-Stephanopoulos, M. Catal. Lett. 2001, 77, 87.

[83] R.R. Salunkhe, V.R. Shinde and C.D. Lokhande, Sens. Actuators B: Chem., 133, 296–301 (2008).

[84] F. Yakuphanoglu, Appl. Surf. Sci., 257, 1413–1419 (2010)

[85]. Chen, K.C., Wang, C.W., Lee, Y.I. & Liu, H.G. 2011. Nanoplates and nanostars of β-PbO formed at the air/water interface. Colloids Surf. A. 373(1-3): 124-129.

[8 6]. Xi G., Peng Y., Xu L., Zhang M., Yu W., Qian Y. (2004). Selected-control synthesis of PbO2 submicrometer- sized hollow spheres and Pb3O4 microtubes. Inorg. Chem. Commun., 7: 607-610.

[87]. Karami H, Karami MA, Haghdar S (2008). Synthesis of uniform nanostructured lead oxide by sonochemical method and its application as cathode and anode of lead-acid batteries. Mater. Res. Bull., 43: 3054-3065.

[88]. Ansari, S. G., P. Boroojerdian, S. K. Kulkarni, S. R. Sainkar, R. N. Karekar, and R. C. Aiyer. "Effect of thickness on H 2 gas sensitivity of SnO 2 nanoparticle-based thick film resistors." *Journal of Materials Science: Materials in Electronics* 7 (1996): 267-270.

[89]. Mythili, N., and K. T. Arulmozhi. "Influence of Zinc doping on the structural and optical properties of chemically synthesized PbO nanocrystals." *Optoelectronics and Advanced Materials-Rapid Communications* 8, no. March-April 2014 (2014): 221-224.

[90]. Thirumoorthi, M., and J. Thomas Joseph Prakash. "A study of Tin doping effects on physical properties of CdO thin films prepared by sol–gel spin coating method." *Journal of Asian Ceramic Societies* 4, no. 1 (2016): 39-45.

[91]. Licurgo, J. S. C., G. R. de Almeida Neto, and H. R. Paes Junior. "Structural, electrical and optical properties of copper-doped zinc oxide films deposited by spray pyrolysis." *Cerâmica* 66 (2020): 284-290.

[92]. Suryawanshi, V. N., Ashwini S. Varpe, and Mrinalini D. Deshpande. "The influence of rare earth (RE) dopants on structural, optical and gas sensing properties of spray deposited PbO thin films, where RE= Ce, Nd and Eu." *Pramana* 96, no. 1 (2022): 38.

[93] Mengting Liu, Qiuquang Zhan, Wei Li, Rui Lei, Qinyu He and Yinzhen Wang, Journal of Alloys and Compounds 792, 1000 (2019).

[94] Mehmood F, Iqbal J, Jan T, Gul A, Mansoor Q and Faryal R 2017 Structural, photoluminescence, electrical, anti-cancer and visible light driven photocatalytic characteristics of Co doped WO3 nanoplatesVib. Spectrosc. 93 78–89

[95] L. M. Droessler, H. E. Assender, A. R. Watt, Thermally deposited lead oxides for thin film photovoltaics, Materials Letters 71 (2012) 51

[96] M. Suganya, N. Narasimman, H. J. Srivind, V. S. Nagarethinam, K. Usharani, A. R. Balu, Studies on the physical properties of spray and silar deposited lead oxide thin films, J. Electron Devices 21 (2015) 1842.

[97] M. Suganya, A. R. Balu, K. Usharani, Role of substrate temperature on the growth mechanism and physical properties of spray deposited lead oxide thin films, Materials Science-Poland 32 (3) (2014) 448.

[98]. Khan, M. M., Khan, M. W., Alhoshan, M., AlSalhi, M. & Aldwayyan, A. Infuences of Co doping on the structural and optical properties of ZnO nanostructured. Appl. Phys. A 100(1), 45–51 (2010).

[99]. Ren, T., Baker, H. R. & Poduska, K. M. Optical absorption edge shifs in electrodeposited ZnO thin flms. Tin Solid Films 515(20–21), 7976–7983 (2017)

[100] Meenakshi M, Gowthami V, Perumal P and Sanjeeviraja C 2014 Effect of RF power on the structuraland optical characterization of (WO3) 0.90 (V2O5) 0.10 thin filmsInt. J. ChemTech. Res. 6 5412–8.

[101]. Boon-on, Patsorn, Cing-Ru Chiang, Raja Rajendran, Nipapon Suriyawong, Jen-Bin Shi, and Ming-Way Lee. "Pb5Sb8Se17-δ nanocrystals: A new solar absorber material with an optimal bandgap and an efficiency near 6% under 0.05 sun." *Journal of Power Sources* 485 (2021): 229324.

[102] Mehmood F, Iqbal J, Jan T and Mansoor Q 2017 Structural, Raman and photoluminescence properties of Fe doped WO3 nanoplates with anti-cancer and visible light driven photocatalytic activitiesJ. Alloys Compd. 728 1329–37